Two-dimensional model simulations of interannual variability in the tropical stratosphere

Eric L. Fleming,[1] Charles H. Jackman, David B. Considine,[2], and Joan Rosenfield,[3]
NASA Goddard Space Flight Center, Greenbelt, Maryland

Received _____; accepted _____

Submitted version: July 23, 2001

To be Submitted to Journal of Geophysical Research

Short title: 2-D MODEL SIMULATIONS OF INTERANNUAL VARIABILITY

[1]Also at Science Systems and Applications, Inc., Lanham, Maryland.

[2]Also at Department of Meteorology, University of Maryland, College Park.

[3]Also at UMBC, Baltimore, Maryland.

Abstract.

Meteorological data from the United Kingdom Meteorological Office (UKMO) and constituent data from the Upper Atmospheric Research Satellite (UARS) are used to construct yearly zonal mean dynamical fields for the 1990s for use in the GSFC 2-D chemistry and transport model. This allows for interannual dynamical variability to be included in the model constituent simulations. In this study, we focus on the tropical stratosphere. We find that the phase of quasi-biennial oscillation (QBO) signals in equatorial CH_4, and profile and total column O_3 data is resolved quite well using this empirically-based 2-D model transport framework. However, the QBO amplitudes in the model constituents are systematically underestimated relative to the observations at most levels. This deficiency is probably due in part to the limited vertical resolutions of the 2-D model and the UKMO and UARS input data sets. We find that using different heating rate calculations in the model affects the interannual and QBO amplitudes in the constituent fields, but has little impact on the phase. Sensitivity tests reveal that the QBO in transport dominates the ozone interannual variability in the lower stratosphere, with the effect of the temperature QBO being dominant in the upper stratosphere via the strong temperature dependence of the ozone loss reaction rates. We also find that the QBO in odd nitrogen radicals, which is caused by the QBO modulated transport of NO_y, plays a significant but not dominant role in determining the ozone QBO variability in the middle stratosphere. The model mean age of air is in good overall agreement with that determined from tropical lower-middle stratospheric OMS balloon observations of SF_6 and CO_2. The interannual variability of the equatorial mean age in the model increases with altitude and maximizes near 40 km, with a range of 4-5 years over the 1993-2000 time period.

1. Introduction

The quasi-biennial oscillation (QBO) is the dominant mode of interannual variability in the tropical lower stratosphere. Since its discovery by *Reed et al.* [1961] and *Veryard and Ebdon* [1961], there have been numerous observational studies documenting the QBO in zonal wind and temperture [e.g., *Reed*, 1964; *Angell and Korshover*, 1970; *Dunkerton and Delisi*, 1985; *Naujokat*, 1986; *Nash*, 1988; *Ortland et al.*, 1996; *Randel et al.*, 1999]. The QBO is believed to be generated by dissipation of vertically propagating equatorial waves [e.g., *Lindzen and Holton*, 1968; *Holton and Lindzen*, 1972], although recent analysis has suggested that gravity waves can contribute significantly to the forcing of the QBO westerly phase [*Alexander and Vincent*, 2000]. The associated QBO signal in the meridional circulation gives rise to a QBO variation in ozone and long lived trace species [e.g., *Hasebe*, 1994; *Eluszkiewicz et al.*, 1996; *Cordero et al.*, 1997; *O'Sullivan and Dunkerton*, 1997; *Randel et al.*, 1998]. Additionally, the effect of the QBO on the circulation and constituent distributions in the extratropics has been investigated in a variety of studies [e.g., *Holton and Tan*, 1980; *Lait et al.*, 1989; *Bowman*, 1989; *Randel and Cobb*, 1994; *Tung and Yang*, 1994; *O'Sullivan and Dunkerton*, 1997; *Gray and Russell*, 1999; *Randel et al.*, 1998; *Kinnersley and Tung*, 1999; *Randel et al.*, 1999].

The tropical upper stratosphere is characterized by a dominant semi-annual oscillation (SAO) signal in wind and temperature [e.g., *Garcia et al.*, 1997 and references therein], and long lived tracers [e.g., *Choi and Holton*, 1991; *Randel et al.*, 1994]. The upper stratospheric SAO in the circulation and tracer distributions are also thought to be modulated by the QBO variations in the underlying lower stratospheric winds [e.g., *Ruth et al.*, 1997; *Kennaugh et al.*, 1997].

Various modeling studies have investigated the processes that control the QBO and SAO responses in stratospheric ozone and constituent distributions. *Gray and Pyle*, [1987] used an interactive 2-D model with a parameterization of momentum transfer to

the zonal flow from dissipating equatorial Kelvin waves to examine the stratospheric semi-annual oscillation. Their model qualitatively reproduced a SAO in zonal wind, and a "double peaked" structure in the tracer fields associated with the SAO meridional circulation. These authors extended this work to include parameterizations of Kelvin and Rossby-Gravity waves associated with the lower stratospheric QBO [*Gray and Pyle*, 1989]. Although their simulations did not correspond to a particular time period and generated a near constant QBO period, they were able to reproduce many qualitative aspects of the QBO in zonal wind, temperature, and total ozone. *Gray and Dunkerton* [1990] then investigated the interaction of the QBO with the seasonal cycles in each hemisphere, and successfully reproduced several of the basic features of the ozone QBO in the tropics and subtropics in their 2-D interactive model. Subsequent studies discussed the QBO signal in various trace gases generated in the model simulations [*Gray and Chipperfield*, 1990; *Chipperfield and Gray*, 1992].

Gray and Ruth [1993] followed these investigations by simulating a QBO in their 2-D model for the specific years 1971-1990 by relaxing the model equatorial winds to observations. The resulting QBO signal in the total ozone simulation agreed reasonably well with satellite observations. These authors also discussed the importance of the QBO interaction with the annual cycle in determination of the ozone anomalies in the subtropics. In a related study, *Jones et al.* [1998] used a 2-D interactive model to investigate the QBO and seasonal dependence on the tracer transport in the tropics and subtropics.

Simulations of QBO variations have also been recently performed using 3-D models. *Nagashima et al.* [1998] simulated a QBO in ozone using a general circulation model (GCM). The resulting model amplitude of the lower stratospheric ozone QBO was somewhat less than observed, with a mostly realistic phase reversal of the signal in the upper stratosphere. *Hamilton et al.* [1999], using high vertical resolution in the GFDL SKIHI GCM, obtained a spontaneous, internally generated oscillation in the equatorial

stratospheric zonal winds which closely resembled a QBO-type oscillation, but with a period less than half of the observed QBO.

The interaction of the QBO and SAO has also been investigated by *Kennaugh et al.* [1997] using a 2-D isentropic model. They found that the lower stratospheric QBO modulates the strength of the upper stratospheric SAO circulation, consistent with the interannual changes seen in CH_4 measurements made by the Halogen Occultation Experiment (HALOE) onboard the Upper Atmospheric Research Satellite (UARS). These authors discuss the subtle ways in which the time-integrated vertical motion affects the depth of the double-peaked structure in upper stratospheric CH_4.

Our 2-D chemistry and transport model at NASA/Goddard Space Flight Center (GSFC) has been widely used in scientific and assessment studies of the long term changes in stratospheric ozone [e.g., *Jackman et al.*, 1996; *WMO*, 1999]. Incorporating interannual dynamical variability in the model is important to more fully understand past ozone changes and the future ozone recovery [*Jackman et al.*, 1996; *WMO*, 1999; *Chipperfield*, 1999]. We previously examined the impact of interannual variability on our model ozone field using an earlier version of the model transport formulation [*Jackman et al.*, 1991]. This model was able to simulate a good deal of the interannual variability in upper stratospheric ozone at low to middle latitudes where temperature dependent photochemistry controls the ozone distribution. However, this previous model did not resolve the observed QBO in total column ozone.

We have recently upgraded the formulation for deriving our empirical 2-D model transport fields from meteorological data sets. For climatological conditions, this new methodology gives good model agreement with a variety of ozone and long lived tracer measurements [*Fleming et al.*, 1999]. In light of this, we have extended the new formulation to allow for interannual dynamical variations in the model simulations. For this we use the global winds and temperatures from the United Kingdom Meteorological Office (UKMO) data assimilation system for the specific years 1992-2000. Recent

analysis has shown that the UKMO data provide a good representation of the QBO and SAO features in the tropical stratosphere, as well as QBO features in the extratropics during the 1990s [Randel *et al.*, 1999]. Our modeling approach for including interannual variability differs from previous interactive 2-D model studies, e.g., those that imposed a QBO by relaxing the model lower stratospheric equatorial winds to observations and allowing the model circulation to respond globally [e.g., *Gray and Ruth*, 1993; *Kinnersley and Tung*, 1999], or studies that additionally imposed extratropical interannual variability by forcing the model with the observed planetary wave heights at the tropopause [*Kinnersley and Tung*, 1998].

In the present paper, we focus on the tropical stratosphere where the zonal mean constituent distributions are controlled primarily by the residual circulation with eddy diffusion processes being much less important. Previous analysis has shown that in this region, our empirically-based climatological 2-D model framework does a good job in simulating the age of air and seasonal cycle propagation [*Hall et al.*, 1999; *Fleming et al.*, 1999]. Here we extend this analysis to interannual time scales and examine how much of the observed year to year constituent variability in the tropics can be explained in our model utilizing the UKMO meteorological data. We specifically examine the modeled QBO signatures in ozone and CH_4 fields, and how these compare with UARS and TOMS data. We will also examine the relative roles of transport and temperature dependent photochemistry in controlling the tropical ozone changes in the lower and upper stratosphere.

2. GSFC 2-D Model

The GSFC 2-D model has been described previously [*Douglass et al.*, 1989; *Jackman et al.*, 1990; *Considine et al.*, 1994; *Jackman et al.*, 1996]. Our current model has been updated to the latest Jet Propulsion Laboratory (JPL) 2000 recommendations for the gas phase reaction rates and photolysis cross sections [*Sander et al.*, 2000]. The model

climatological transport formulation is discussed in detail in *Fleming et al.* [1999]. Here we provide a brief overview of the analogous application to interannually varying meteorological conditions for the stratosphere based on the 3-D UKMO assimilated winds and temperatures for 1992-2000. As with previous model versions, the current transport for the mesosphere above 1 mbar is climatological and is derived from the CIRA-86 zonal mean and planetary wave reference atmospheres [*Fleming et al.*, 1990; *Barnett and Labitzke*, 1990].

Following the methodology originally formulated by *Garcia and Solomon* [1983], a meridional stream function is calculated to obtain the transformed Eulerian mean circulation $(\bar{v}^*, \bar{w}^*)$. The stream function is derived from: (1) the zonal mean temperatures and zonal winds; (2) the vertical gradient of the mechanical forcing from planetary- and synoptic-scale waves, gravity waves, and equatorial Kelvin and Rossby-Gravity waves; and (3) the latitudinal gradient of the total heating rate which is comprised of diabatic, latent, and net eddy heating.

The planetary- and synoptic-scale wave forcing are proportional to the Eliassen-Palm (E-P) flux divergence [e.g., *Andrews et al.*, 1987] computed from the UKMO winds and temperatures. Momentum forcing from thermally damped equatorial Kelvin and Rossby-Gravity waves is computed using the parameterization discussed in *Gray and Pyle*, [1989]. Gravity wave forcing above 10 mbar is computed from the parameterization of *Lindzen* [1981] and *Holton and Zhu* [1984], using the background zonal mean temperature and zonal wind fields to diagnose the monthly, latitudinal, and vertical distributions of gravity wave drag and diffusion based on a given set of fixed gravity wave parameters. The computed gravity wave drag and diffusion in the stratosphere will undergo interannual variations due to the varying background UKMO zonal wind field. However since the background winds in the mesosphere are climatological, the resulting wave drag and diffusion computed above 1 mbar changes very little from year to year, with only a small interannual component due to the yearly changing background winds

in the stratosphere.

The diabatic heating rates are computed following *Rosenfield et al.* [1994], using the interannually varying UKMO temperatures and HALOE ozone and water vapor. As discussed in the next section, we will show results using both climatological and interannually varying HALOE ozone and water vapor fields in the diabatic heating rate calculations. We do not account for the radiative effects of the anomolous stratospheric aerosol loading during 1991-1992 caused by the Mt. Pinatubo volcanic eruption. However, this should not strongly impact the QBO signals of concern in the present study. Latent heating rates for the troposphere are climatological and are based on *Newell et al.* [1974]. Net gravity wave heating is computed following *Schoeberl et al.* [1983] and *Huang and Smith* [1991], utilizing the vertical diffusion rates computed from the gravity wave parameterization discussed above. Eddy heating from planetary- and synoptic-scale waves [e.g., *Andrews et al.*, 1987] is computed from the UKMO 3-D meteorological fields.

Following *Randel and Garcia* [1994], latitudinal eddy diffusion (K_{yy}) due to planetary- and synoptic-scale wave dissipation is computed self-consistently with the circulation and is taken as the ratio of the E-P flux divergence to the latitudinal gradient of zonal mean potential vorticity. The model vertical eddy diffusion (K_{zz}) in the troposphere and lower stratosphere below 10 mbar is derived from the Brunt-Väisälä frequency squared as computed from the UKMO temperatures. K_{zz} in the mesosphere and upper stratosphere above 10 mbar is obtained from the gravity wave parameterization discussed above.

3. Tropical Dynamical Variability

Randel et al. [1999] previously presented a detailed analysis of the zonal mean interannual and QBO dynamical features derived on a global basis from the UKMO data. In this section, we present a brief overview of the interannual dynamical variability

in the tropical stratosphere derived from the UKMO data for use in our 2-D model.

To examine the relative impact on the model constituents of interannual variations in the advective circulation and eddy diffusion fields, we ran a simulation in which K_{zz} was set to climatology with the circulation and K_{yy} fields varied interannually. We also ran an analogous simulation in which the K_{yy} field was set to climatology with the circulation and K_{zz} fields varied interannually. We found that interannual changes in K_{zz} have a negligible effect on the model constituent simulations in the tropical stratosphere. Interannual changes in K_{yy} have a relatively small impact on the model CH_4 distribution, but have virtually no effect on the profile and total ozone simulations. Therefore in this study, we will focus on the interannual variations in the vertical velocity field of the residual circulation ($\bar{w}^*$) which control the zonal mean constituent distributions in the tropics. In our diagnostic model formulation, the diabatic heating rates dominate the forcing of $\bar{w}^*$ in the equatorial region. The momentum forcing from tropical Kelvin and Rossby-Gravity waves and extratropical planetary waves has a much smaller impact on the model circulation and constituent simulations. In the following sections, we will discuss the sensitivity of the model results to different heating rate calculations.

Figure 1 shows equatorial time series of our computed $\bar{w}^*$ for 1992-2000 at 3 stratospheric levels. Here we show the heating rate calculation in which the temperature, ozone, and water vapor fields all change interannually. This is scenario A as listed in Table 1. Well known features are illustrated in Figure 1, such as the strong QBO signature in lower stratosphere and the dominant SAO in the upper stratosphere, with a transition between the two regimes in the middle stratosphere. The upper stratospheric time series at 3 mbar also shows typically stronger upwelling during the NH winter compared to the SH winter. This is consistent with the stronger dynamical forcing during NH winter, which also produces stronger tropical easterlies [e.g., *Garcia et al.*, 1997]. Figure 1 also reveals a strong interannual component at all levels, and it appears

that the QBO modulates the SAO circulation in the upper stratosphere. This is more clearly seen in the time-height section in Figure 2 (top) in which the trend and seasonal cycles in the $\bar{w}^*$ time series have been removed by regression analysis. Maximum anomaly amplitudes are on the order of ± 0.5 mms^{-1}, with a characteristic downward propagation feature evident.

To isolate the QBO signal in the $\bar{w}^*$ anomaly field, we follow the methodology outlined previously [*Wallace et al.*, 1993; *Randel and Wu*, 1996; *Randel et al.*, 1999]. The interannual anomalies are fit with a linear regression containing the two leading empiricial orthogonal functions (EOFs) of the zonal wind QBO reference time series. This time series is derived from optimal linear combinations of near-equatorial radiosonde observations of zonal wind for 70-10 mbar. Together, these two leading EOFs explain more than 90% of the QBO zonal wind variance for 1956-1990 [*Wallace et al.*, 1993; *Randel et al.*, 1999]. This technique therefore isolates time variations in $\bar{w}^*$ (or other parameters) that are coherent with the lower stratospheric zonal wind QBO. Figure 2 (bottom) shows the resulting QBO fit of $\bar{w}^*$, which captures a significant amount of the interannual variability in $\bar{w}^*$. An out-of-phase relationship between the upper and lower stratosphere is also evident.

The equivalent harmonic amplitude and phase of the QBO signal in $\bar{w}^*$ from scenario A are shown in Figure 3 (solid lines). These are computed from the two leading EOFs shown in Figure 2 (bottom), in a similar fashion to the methodology outlined in *Wallace et al.* [1993]. The QBO amplitude maximizes at ~ 0.2 mms^{-1} in the middle and upper stratosphere between 32 and 42 km. There is a sharp dropoff in amplitude above and below this layer. The phase plot in Figure 3 (plotted in fractional QBO cycle) shows the characteristic downward propagation, with a near 180° phase shift (0.5 cycle) between 3 mbar and 30 mbar.

Our results in Figure 2 are similar to the radiatively determined $\bar{w}^*$ of *Randel et al.* [1999], with a strong correlation between the $\bar{w}^*$ field, the temperature variations, and

the net diabatic heating rates in the tropical stratosphere. We find that our computed $\bar{w}^*$ anomalies are anticorrelated with and slightly preceed, by 1-2 months, our 2-D model ozone (section 4.2) and UKMO temperature anomalies at 20-40 mbar. Our $\bar{w}^*$ results appear to be grossly consistent with the lower stratospheric vertical velocities inferred from the ascent rates of HALOE equatorial $2CH_4 + H_2O$ [*Niwano and Shiotani*, 2001]. These authors report that the positive QBO variations in ascent rates preceed the negative anomalies in temperature and ozone by 2-3 months at 30-60 mbar. However, they also suggest that the QBO variation in their derived ascent rates may be larger than that determined from radiative calculations.

Figure 3 shows results from two additional heating rate calculations. Scenario B (dashed-dotted line) uses the interannually changing UKMO temperatures, but with climatological (1993-2000 average) distributions of ozone and water vapor from HALOE. The resulting $\bar{w}^*$ QBO signal is consistent with the findings of *Randel et al.* [1999]. Using climatological O_3 and H_2O in the heating rates enhances the $\bar{w}^*$ QBO amplitude in the lower stratosphere below 28 km, and decreases the amplitude above 28 km, especially at 35-43 km. Scenario B also results in a secondary maximum near 24 km. The difference in the heating calculations between scenarios A and B is primarily due to the variations in ozone heating. In the lower stratosphere where the temperature and ozone changes are in phase, the net heating due to the QBO ozone anomalies tend to cancel the effect of the QBO-induced circulation, i.e., downward motion (relative to the mean) gives positive ozone anomalies resulting in enhanced heating and enhanced upward motion. The opposite occurs in the upper stratosphere where the QBO-induced circulation results in ozone anomalies that have a positive feedback on the radiative heating and vertical velocity fields, i.e., relative downward motion gives negative ozone anomalies which decreases the heating and enhances the downward motion. The radiative effects of interannual changes in ozone therefore decrease the interannual and QBO variations in $\bar{w}^*$ below $\sim$28 km and enhance the variations above $\sim$28 km. However, the QBO

phase in Figure 3 changes very little between scenarios A and B.

Comparisons with Singapore rawinsonde data suggest that the UKMO temperatures underestimate the QBO amplitude by at least 40% [*Randel et al.*, 1999]. This would result in an underestimation of the QBO amplitude in the computed radiative heating rates and $\bar{w}^*$ in the equatorial stratosphere. *Randel et al.* [1999] found that increasing the QBO temperature anomalies in the UKMO data by 40% substantially increased the corresponding amplitude in their derived $\bar{w}^*$ in the lower stratosphere, with a smaller effect in the upper stratosphere. To understand how such a bias might affect our model constituent simulations, we made a similar heating rate and $\bar{w}^*$ calculation in which the QBO amplitude in the UKMO temperatures was increased by 40% (scenario C). The O_3 and H_2O in this scenario were varied interannully as in scenario A. The resulting QBO signal in $\bar{w}^*$ (Figure 3, dotted line) is enhanced significantly throughout most of the equatorial stratosphere compared to scenario A (solid line). As with scenario B, the QBO phase in $\bar{w}^*$ exhibits only negligible changes between scenarios A and C in Figure 3. In the following sections, we will discuss how the different heating rate and $\bar{w}^*$ calculations in scenarios A, B, and C affect the model simulated interannual constituent variations.

4. Model constituent simulations

We now compare the model simulated interannual changes in equatorial CH_4 and ozone with UARS and TOMS observations. We will show results from scenarios A, B, and C described in section 3. We will also discuss the relative influence of interannual changes in transport, temperature, and odd nitrogen photochemistry on the resulting ozone simulations.

All results are taken from simulations in which the model was run for 41 years using 1960-2000 time dependent source gas boundary conditions from *WMO* [1999]. For years corresponding to 1960-1992, the simulations use the 1992 UKMO-derived transport

fields repeated each year, with the UKMO-derived transport for each particular year then used for 1993-2000. We note that long term variability introduced by the 11-year cycle in solar UV flux was not included in the model simulations.

Because we use the 1992 dynamics for all years prior to 1992 instead of the actual yearly dynamics which are not available, it is important to estimate the possible bias introduced by the model's "memory" of the initial conditions. To do this we ran a simulation using the 1993 dynamics repeated each year for 1960-1993, with the proper yearly dynamics then used for 1994-2000. We also ran an analogous simulation using the 1994 dynamics. We found that the model in the tropics has a spin-up time of about 1 year, i.e., it takes 1 year for the model to adjust to different initial conditions caused by the different dynamical fields. Therefore in the following sections, we omit the 1992 results and show only the constituent simulations for 1993-2000. This also avoids the problems with UARS data contamination and other complicating factors caused by the anomolous Pinatubo aerosol loading during 1991-1992.

4.1. CH_4

Figure 4 compares time series of equatorial (10°S-10°N) HALOE v19 monthly mean CH_4 along with the model simulations at three stratospheric levels. The model results from the three heating rate calculations (scenarios A, B, and C) show only small differences, and these will be discussed below. The HALOE data show generally weak seasonal and interannual cycles in the lower stratosphere. The amplitudes of these variations increase with altitude, coincident with the increase in the vertical gradient of methane [e.g., *Cordero et al.*, 1997]. The model simulations qualitatively mimic this altitude variation, and are able to match the phase of the seasonal cycles in the HALOE data quite well in the middle and upper stratosphere. The model-data agreement in the absolute value of CH_4 is especially good in the middle and upper stratosphere throughout the time period. The simulations at 21 mbar reveal a small underestimation

of about 0.05 ppmv in the absolute amount of CH_4 after 1995. This deficiency is likely due to a model underestimation of the mean tropical upwelling in the lower stratosphere, resulting in too little CH_4 transported up from the troposphere.

The interannual changes in the model and HALOE CH_4 are more clearly seen in Figure 5, which shows the time series with the trend and seasonal cycles removed by regression analysis (a solar cycle component has also been removed from the HALOE data). Such interannual variations have previously been investigated in the UARS long-lived tracer data [*Cordero et al.*, 1997; *O'Sullivan and Dunkerton*, 1997; *Randel et al.*, 1998]. The models appear to track the QBO-type changes in the data reasonably well throughout the time period, including the phase of the QBO variation in the lower and upper stratosphere. Although some of the shorter-term oscillations seen in the data are not as well resolved in the model at 10 and 21 mbar.

Vertical profiles of the amplitude and phase of the methane QBO signal are shown in Figure 6. These were computed following the same methodology used for the $\bar{w}^*$ field (Figure 3) as discussed in section 3. The models capture the general altitudinal variation of the HALOE amplitude, with a sharp upper stratospheric maximum centered at 3 mbar (40 km) coincident with the strongest vertical gradient in CH_4, a minimum near 10 mbar, and secondary maximum near 20 mbar. All three models are similar in phase (Figure 6, bottom panel), and resolve fairly well the altitudinal phase variation of the observations. There is some model discrepancy in phase at the very lower and upper levels where the amplitudes are quite weak.

Figures 4-6 show that model scenario A (solid line) tends to underestimate the QBO amplitude at most heights, with a difference of 25-30% at 40 km. Including climatological O_3 and H_2O in the heating rates (scenario B, dashed-dotted line) affects the CH_4 amplitude in a manner consistent with the $\bar{w}^*$ field (Figure 3), i.e., the amplitude increases in the lower stratosphere below 35 km, and decreases in the upper stratosphere at 38-43 km, although the CH_4 amplitude decrease near 40 km appears to

be smaller than the relative decrease in $\bar{w}^*$ seen in Figure 3. Scenario B provides better agreement with the HALOE amplitude between 10 and 20 mbar, but slightly worsens the comparison at 40 km. As expected, increasing the QBO temperature anomalies in the heating rates (scenario C, dotted line) increases the QBO CH_4 amplitude throughout the stratosphere to be closer to the HALOE data. The improvement is especially noticeable in the region of the 40 km maximum. Among the three models, scenario C appears to provide the best overall agreement with the HALOE CH_4 data in Figure 6.

We note finally that the QBO response will be similar for other long lived tracers with similar vertical gradients [*Cordero et al.*, 1997]. For example as with CH_4, the vertical gradient in HF is weak in the lower stratosphere and strong in the upper stratosphere. The model and HALOE QBO responses in HF (not shown) are weak in the lower stratosphere and have sharp maxima in the upper stratosphere near 40 km, but are 180° out of phase with the QBO responses in CH_4 due to the reversed orientation of the vertical gradients of the two constituents.

4.2. Profile Ozone

Figure 7 shows time series for 1993-2000 of ozone from the UARS Microwave Limb Sounder (MLS) v5 and HALOE v19 and the model simulations at 3 stratospheric levels. The time series with the trend and seasonal cycles removed via regression analysis are shown in Figure 8 (again a solar cycle component has also been removed from the HALOE and MLS data). Note the MLS data is only available through June 1997. Because of the sharp vertical gradients in ozone, there is a strong QBO signal in the lower stratosphere, with a transition to a dominant SAO in the middle and upper stratosphere in both the model and data. The model tracks the phase of the seasonal and interannual signals in the UARS data fairly well. A strong QBO-type feature is seen at all levels of the stratosphere in the HALOE and MLS data, and the model agrees qualitatively with these observations. Also, both the modeled and observed ozone

in the upper stratosphere have a well-known strong anticorrelation with temperature, on both seasonal and interannual time scales. In the lower stratosphere, the modeled and observed ozone have a strong positive correlation with temperature seasonally and interannually, and both ozone and temperature are anti-correlated with the $\bar{w}^*$ field, with a slight phase lag of 1-2 months. As with methane, the differences among the three model scenarios in Figures 7 and 8 are relatively small, as will be discussed below.

The model simulations in Figure 7 systematically overestimate the observations by 0.55 ppmv in the lower stratosphere where ozone is controlled by transport. Since the MLS and HALOE data agree quite well, we suspect that this bias is caused by the model underestimating the mean upwelling in the tropics causing higher ozone concentrations than observed. This is consistent with Figure 4 in which overly weak model upwelling caused an underestimation of CH_4 relative to the data. As ozone becomes increasingly less influenced by transport with increasing altitude, this bias becomes very small in the middle stratosphere. The model underestimation of the data in the upper stratosphere in Figure 7 is due to the well-known ozone deficit problem [e.g., *Minschwaner et al.*, 1993; *Eluszkiewicz and Allen*, 1993; *Dessler et al.*, 1996] as discussed in our previous work [*Jackman et al.*, 1996]. This deficiency has been reduced somewhat in the present model simulations that include the reaction $ClO + OH- > HCl + O_2$ [*Sander et al.*, 2000]. The current model scenarios systematically underpredict the HALOE O_3 by 0.75 ppmv (11%) at 3 mbar.

Equatorial time-height sections of the QBO fits to the detrended and deseasonalized ozone time series from UARS and model scenario A are shown in Figure 9. The QBO signal explains a significant amount of the interannual variability in both the model and data. For the most part, the model reveals good qualitative consistency with the data, showing a strong downward propagation characteristic from the upper to the lower stratosphere.

The corresponding amplitudes and phases of the QBO fits for the UARS data and

model scenarios A, B, and C are shown in Figure 10. As with the CH_4 comparisons, the models capture quite well the altitudinal phase change below 45 km where the QBO amplitude is significant. Model scenario A (solid line) shows some general consistency with the data in the amplitude variation with altitude, i.e., maxima near 25 and 35 km, with a minimum in between. However below 40 km, the magnitude of the QBO amplitude is systematically underestimated in the model by as much as a factor of 2. Consistent with $\bar{w}^*$, the ozone QBO amplitude in scenario B (dashed-dotted line in Figures 7, 8, and 10) is enhanced (diminished) below (above) 28 km compared to scenario A. However, the differences between the two heating rate calculations become much less apparent above 35 km as ozone becomes increasingly controlled by photochemistry. The model QBO ozone amplitude in scenario C (in which the QBO temperture anomalies have been increased by 40%) is generally closer to the HALOE data than scenario A, but still underestimates the observed amplitude at most altitudes. The change in the modeled ozone in the lower stratosphere in scenario C is primarily due to the vertical velocity enhancements, with the upper stratospheric model ozone changes due mainly via the temperature dependent reaction rates.

To further investigate the processes controlling the interannual ozone variations, we ran two additional model simulations listed in Table 1. In scenario D, the transport was allowed to vary interannually as in scenario A, but the temperatures in the photochemistry were set to climatological values. The opposite case (climatological transport, interannual temperatures in the photochemistry) was done in scenario E. The resulting detrended and deseasonalized O_3 time series are shown in Figure 11, and the corresponding QBO amplitude and phase are shown in Figure 12. Transport almost completely determines the total interannual signal below 30 mbar, as scenario D (red line) is nearly identical to scenario A (black line). Scenario E (blue line), which has only the interannual temperature dependent photochemistry with transport being climatological, exhibits very small interannual variability below 30 mbar. Transport

and photochemistry have similar contributions to the ozone variability in the middle stratosphere, with photochemistry becoming dominant in the upper stratosphere above about 4 mbar.

Below about 20 mbar, the transport-induced interannual signal is out of phase with the temperature effect, as downward motion (relative to the mean) in the lower stratosphere increases ozone directly, but also creates warmer temperatures which decreases ozone photochemically. This is seen in the time series at 31 mbar in Figure 11 (bottom panel), and by the fact the QBO signal in scenario E is one-half cycle out of phase with scenarios A and D in the lower stratosphere (Figure 12, bottom panel). This is also illustrated by the fact that the QBO amplitude in scenario D somewhat exceeds that of the full interannual simulation (scenario A) in the lower stratosphere (Figure 12, top panel). This out-of-phase relationship diminishes with height as the temperature impact on ozone reinforces that of transport above about 10 mbar.

In a previous analysis of the QBO signal in O_3, *Chipperfield et al.* [1994] concluded that the QBO modulation of NO_2, via the modulated transport of NO_y, is the major cause of the ozone QBO signal above 30 km, with the temperature QBO effect on the ozone reaction rates being very minor. Their results were in contrast to other studies who concluded that the upper stratospheric ozone QBO signal was caused by the temperature QBO influencing the ozone loss rates [e.g., *Ling and London*, 1986; *Zawodny and McCormick*, 1991].

To test these hypotheses in our model, we ran an additional simulation (F) in which all odd nitrogen species (N, NO, NO_2, NO_3, N_2O_5, HNO_3, $ClONO_2$, $BrONO_2$, HO_2NO_2) were held constant throughout the run (the transport and temperature were both varied interannually as in scenario A). The resulting ozone time series and QBO signal are depicted by the purple dashed-dotted lines in Figures 11 and 12. This simulation reveals that without the QBO signal in NO_y and NO_x, the QBO in ozone has been reduced in the middle stratosphere at 25-40 km. The largest reduction, by a factor of two, occurs

near 10 mbar. However, the ozone signal is still substantial at this level, indicating that the temperature QBO effect on the ozone loss rates (other than the NO_x-induced loss) and transport, contribute significantly to the ozone interannual variability in the middle stratosphere. Figures 11 and 12 also illustrate that the non-NO_x temperature dependent photochemistry is the dominant process in driving the ozone QBO signal in the upper stratosphere at and above 3 mbar. This is revealed by the fact that keeping the NO_x species constant in scenario F has only a very small effect on the interannual ozone signal at these levels. These results are consistent with the findings of *Ling and London* [1986] and *Zawodny and McCormick* [1991], but appear to be somewhat in contrast with the modeling results of *Chipperfield et al.* [1994].

4.3. Total Column Ozone

Figure 13 shows equatorial total column ozone (10°S to 10°N) for 1993-2000 from the new combined TOMS/SBUV merged data set [*Stolarski et al.,* 2001] (red dashed-asterisk line), and model scenarios A (solid line), B (dashed-dotted line), and C (dotted line). The TOMS/SBUV merged data is currently available through March 2000. The unfiltered time series (top panel) shows that the model simulations qualitatively reproduce the phase of the TOMS/SBUV seasonal cycles quite well. Consistent with the vertical profile ozone in the lower stratosphere (Figure 7, bottom), the model systematically overpredicts total ozone by 9 DU relative to TOMS/SBUV. Again this is most likely due to a small underestimation of the strength of the model residual circulation in the lower stratosphere.

The bottom panel in which the trend and seasonal cycles have been removed (a solar cycle component has also been removed from the TOMS/SBUV time series) reveals the well-known QBO signature in equatorial total ozone which has been frequently discussed in previous work [e.g., *Lait et al.,* 1989; *Bowman,* 1989]. As with the seasonal cycles, all 3 model simulations track the phase of the observed total ozone

QBO quite well. This is also shown in Table 2 which lists the QBO amplitude and phase in total ozone (10°S-10°N) from the 6 model scenarios and the TOMS/SBUV data. However, consistent with the CH_4 and profile ozone comparisons, all model simulations underestimate the observed total ozone QBO amplitude. Scenario A (solid line in Figure 13) underestimates the amplitude by a factor of 3. This discrepancy is somewhat improved in scenario C (dotted line) with the QBO temperature anomalies increased by 40%, but this model simulation still underestimates the observed total ozone QBO amplitude by nearly a factor of 2. Scenario B (dashed-dotted line) shows the best comparison with the data, and only slightly underestimates the observed QBO amplitude. This illustrates that the modeled QBO total ozone distribution is rather sensitive to the choice of using either climatological or interannual O_3 variations in the heating rate calculation.

Scenario D, which only has the interannual variability in the transport (temperatures are climatological) reveals a total ozone time series (not shown) and QBO phase (Table 2) very similar to scenario A. However, without the countering effect of the temperature QBO on the reaction rates, scenario D reveals a slightly larger QBO amplitude in total ozone relative to scenario A (Table 2). Including only the temperature variability in scenario E (climatological transport) gives a very weak QBO signal in total ozone which is expectedly 180° of phase with the other scenarios.

We note finally that the QBO total ozone amplitude in the simulation with constant odd nitrogen species (scenario F) is actually increased slightly compared with scenario A, with almost no change in phase (Table 2). This amplitude increase appears to be in conflict with Figure 12 in which scenario F produced a smaller QBO amplitude in the ozone profile at almost all levels compared to scenario A. However, this apparent contradiction can be explained by Figure 9 which illustrates that the interannual variability in ozone is strongly layered in the vertical. A reduction in the QBO amplitude in the middle stratosphere as seen in Figure 12, could therefore lead to

an *increase* in the QBO amplitude in the total column, as is the case with scenario F.

4.4. Age of Air

The mean age of air (Γ) is a widely used transport diagnostic for stratospheric models [e.g., *Hall et al.*, 1999]. The mean age can be determined from an inert tracer with a linearly time increasing tropospheric mixing ratio, such as sulfur hexafluoride (SF_6) or annually averaged CO_2. Figure 14 shows vertical profiles of mean age taken from the tropical tropopause determined from balloon measurements of SF_6 (red triangles) and CO_2 (red plus signs). These data were taken at 7°S during February and November 1997 as part of the Observations of the Middle Stratosphere (OMS) campaign [e.g., *Hall et al.*, 1999]. Figure 14 also includes Γ derived from in situ ER-2 aircraft measurements of SF_6 (blue square) and CO_2 (blue asterisk) at 20 km averaged over several field campaigns during 1992 to 1997 for 10°S-10°N [*Elkins et al.*, 1996; *Boering et al.*, 1996].

The solid line depicts the 1993-2000 average age profile for model simulation A for 10°S-10°N. This average profile is in good overall agreement with the observations throughout the tropical stratosphere, similar to a previous comparison with our climatological model transport [*Fleming et al.*, 1999]. Above the tropopause, the vertical gradient in the average model Γ is slightly weaker than indicated by the data. The model age is slightly older than the observations at 16-23 km, and a bit younger than the data above about 23 km. This likely reflects a small underestimation in the strength of the model tropical upwelling in the lower stratosphere and an overestimation in the middle stratosphere. The lower stratospheric bias in the model $\bar{w}^*$ is consistent with the lower stratospheric comparisons in Figures 4, 7, and 13 in which the model underestimated the observed CH_4 and overestimated the observed profile ozone and total column ozone amounts.

The dotted line in Figure 14 shows the model average Γ for February and November

1997 at 7°S, coincident with the OMS balloon data shown in the Figure. The model bias discussed above is slightly improved in the coincident profile as the model age is slightly older, by 1-2 months, and is closer to the data at 23-30 km. However, this model profile is still a bit younger than the data at 26-30 km.

The dashed lines in Figure 14 depict the range of the model interannual variations at each altitude over 1993-2000, determined from the deseasonalized time series of Γ. The interannual range increases with altitude from near zero at the tropical tropopause to a maximum of 1.0 years at 40 km. At this level, Γ ranges from 4-5 years over the 1993-2000 time period. The average Γ reaches a maximum of 5.6 years with a range of 5.3-6 years just above 60 km, with these values remaining nearly constant with height above this level.

As with the other tracers, there are significant QBO and seasonal signals in Γ. The QBO amplitude distribution with altitude is similar to that of CH_4 (Figure 6), and the seasonal variations in the model Γ are also analogous to those in CH_4 (Figure 4). The largest amplitudes of ± 0.2 years for the QBO signal and ± 0.28 years for the seasonal variations occur near 40 km. However, the variations in Γ are 180° out of phase with those of methane since the vertical gradients of mean age and CH_4 are reversed.

We note finally that the 1993-2000 average equatorial Γ profiles for simulations B and C are very similar to that of model simulation A in Figure 14. However, the interannual age variations in scenario C were slightly larger at all levels than those in scenario A, consistent with the larger variations in equatorial $\bar{w}^*$ seen in Figure 3. For the case of scenario B, the interannual Γ variations were larger than scenario A only below 27 km, again consistent with the variations in $\bar{w}^*$. Above 27 km, the age variability in scenarios A and B are very similar since the vertically integrated differences in the $\bar{w}^*$ QBO amplitudes between the two scenarios (Figure 3) tend to cancel once air parcels have reached the equatorial upper stratosphere.

4. Summary and Conclusions

We have used UKMO meteorological data and UARS constituent data to simulate interannual dynamical variability during the 1990's in our GSFC 2-D stratospheric chemistry and transport model. Since the model is widely used to study the long term changes in stratospheric ozone, incorporating interannual variability in the simulations is important to investigate past ozone changes and the future ozone recovery. In this study, we have focused on the tropical stratosphere where eddy motions are generally weak and the mean upward velocity of the residual circulation is the dominant constituent transport mechanism. Because of this, the empirically-based 2D model framework used here adequately resolves many qualitative features of the seasonal and QBO signatures in tropical stratospheric constituent observations. The phase of the seasonal, interannual, and QBO variations observed in CH_4, and profile and total column O_3 data are captured quite well by the model. We also found that the QBO phase variation with altitude was relatively insensitive to the different heating rate calculations imposed in the model.

Overall, the interannual and QBO amplitudes in the model simulations systematically underestimate the observations at most levels. This amplitude deficiency is particularly acute in the total ozone comparison. The model also did not fully resolve some of the altitudinal structure in the profile ozone QBO amplitude. Using climatological O_3 and H_2O in the heating rates (scenario B) significantly improved this discrepancy in the lower stratosphere. However, this simulation is not as realistic as the base simulation A which includes interannual changes in the temperature, O_3, and H_2O data input into the heating rate calculations.

These model deficiencies in resolving the QBO amplitude are probably due in part to the limited vertical resolutions of both the 2-D model and the input data sets (UKMO, UARS) used in the heating rate and dynamical calculations. The vertical grid spacing is $\sim$2 km in the 2-D model, $\sim$2.7 km for the UARS (level 3A) data, and

~2.5-8 km for the stratospheric UKMO data available at the standard pressure levels. Representation of the QBO signal in the upper stratospheric UKMO analyses is further limited by the fact that the temperatures at the upper levels are largely determined by poor vertical resolution satellite radiances. Lack of proper spatial resolution in the model and input meteorological data would cause the QBO signal to be "smeared out" in the resulting model constituent simulations. Enhancing the QBO temperature amplitudes in the UKMO data to be closer to those observed in the radiosonde data improved the model results in this regard. However, the model constituent QBO signals were still underestimated relative to the UARS data. The fact that radiative calculations may underestimate the QBO variations in the derived $\bar{w}^*$ relative to those derived from trace gas ascent rates [*Niwano and Shiotani*, 2001] could also contribute to the model deficiency in resolving the observed QBO constituent amplitudes.

Sensitivity tests revealed that as expected, the QBO in transport dominates the ozone interannual variability in the lower stratosphere. The effect of the temperature QBO is dominant in the upper stratosphere via the reaction rates that control ozone destruction. Also, the QBO in NO_x, which is caused by the QBO modulated transport of NO_y, plays a significant, but not dominant role in determining the ozone variability in the middle stratosphere between 25 and 40 km. The impact of transport and the non-NO_x temperature dependent ozone loss rates is substantial at these levels.

The equatorial mean age of air in the model averaged over 1993-2000 is in good overall agreement with that determined from lower and middle stratospheric OMS balloon observations of SF_6 and CO_2 taken during 1997. The interannual variability in the model Γ increases with altitude and maximizes near 40 km, with a range of 4-5 years during the 1993-2000 time period. The oldest air occurs at and above 60 km, with an altitudinally independent range of 5.3-6 years during 1993-2000.

Although we have discussed only the results in the tropics in this paper, it is of significant interest to investigate the model simulations of interannual variability in the

subtropics and extratropics. This will be addressed in a future study.

Acknowledgments. We thank D. Waugh, P. Newman, T. Dunkerton, J. Ziemke, and B. Randel for helpful discussions. We also thank the NASA Atmospheric Chemistry Modeling and Analysis Program and the UARS Science Investigation Program for support of this project.

References

Alexander, M.J., and R.A. Vincent, Gravity waves in the tropical lower stratosphere: A model study of seasonal and interannual variability, *J. Geophys. Res., 105*, 17983-17993, 2000.

Andrews, D.G., J.R. Holton, and C.B. Leovy, *Middle Atmosphere Dynamics*, 498 pp., Academic, San Diego, Calif., 1987.

Angell, J.K., and J. Korshover, Quasi-biennial, annual, and semiannual zonal wind and temperature harmonic amplitudes in the stratosphere and low mesosphere of the Northern Hemisphere, *J. Geophys. Res., 75*, 543-550, 1970.

Barnett, J.J., and K. Labitzke, Climatological distribution of planetary waves in the middle atmosphere, *COSPAR International Reference Atmosphere: 1986, Part II: Middle Atmosphere Models, Adv. Space Res., 10, No. 12*, 63-91, 1990.

Boering, K.A., S.C. Wofsy, B.C. Daube, H.R. Schneider, M. Loewenstein, J.R. Podolske, and T.J. Conway, Stratospheric mean ages and transport rates from observations of carbon dioxide and nitrous oxide, *Science, 274*, 1340-1343, 1996.

Bowman, K.P., Global patterns of the quasi-biennial oscillation in total ozone, *J. Atmos. Sci., 46*, 3328-3343, 1989.

Chipperfield, M.J., and L.J. Gray, Two-dimensional model studies of the interannual variability of trace gases in the middle atmosphere, *J. Geophys. Res., 97*, 5963-5980, 1992.

Chipperfield, M.J., L.J. Gray, J.S. Kinnersley, and J. Zawodny, A two-dimensional model study of the QBO signal in SAGE II NO_2 and O_3, *Geophys. Res. Lett., 21*, 589-592, 1994.

Chipperfield, M.J., Multiannual simulations with a three-dimensional chemical transport model, *J. Geophys. Res., 104*, 1781-1805, 1999.

Choi, W.K., and J.R. Holton, Transport of N2O in the stratosphere related to the equatorial semiannual oscillation, *J. Geophys. Res., 96*, 22543-22557, 1991.

Considine, D.B, A.R. Douglass, and C.H. Jackman, Effects of a polar stratospheric cloud parameterization on ozone depletion due to stratospheric aircraft in a two-dimensional model, *J. Geophys. Res., 99*, 18,879-18,894, 1994.

Cordero, E.C., S.R. Kawa, and M.R. Schoeberl. An analysis of tropical transport: Influence of the quasi-biennial oscillation, *J. Geophys. Res., 102*, 16,453-16,461, 1997.

Dessler, A.E., S.R. Kawa, D.B. Considine, J.W. Waters, L. Froidevaux, and J.B. Kumer, UARS measurements of ClO and NO_2 at 40 and 46 km and implications for the model "ozone deficit", *Geophys. Res. Lett., 23*, 339-342, 1996.

Douglass, A.R., C.H. Jackman, R.S. Stolarski, Comparison of model results transporting the odd nitrogen family with results transporting separate odd nitrogen species, *J. Geophys. Res., 94*, 9862-9872, 1989.

Dunkerton, T.J., and D.P. Delisi, Climatology of the equatorial lower stratosphere, *J. Atmos. Sci., 42*, 376-396, 1985.

Elkins, J.W., et al., Airborne gas chromatograph for in situ measurements of long-lived species in the upper troposphere and lower stratosphere, *Geophys. Res. Lett., 23*, 347-350, 1996.

Eluszkiewicz, J., and M. Allen, A global analysis of the ozone deficit in the upper stratosphere and lower mesosphere, *J. Geophys. Res., 98*, 1069-1082, 1993.

Eluszkiewicz, J., et al., Residual circulation in the stratosphere and lower mesosphere as diagnised from microwave limb sounder data, *J. Atmos. Sci., 53*, 217-240, 1996.

Fleming, E.L., S. Chandra, J.J. Barnett, and M. Corney, Zonal mean temperature, pressure, zonal wind, and geopotential height as functions of latitude, *COSPAR International Reference Atmosphere: 1986, Part II: Middle Atmosphere Models, Adv. Space Res., 10, No. 12*, 11-59, 1990.

Fleming, E.L., C.H. Jackman, R.S. Stolarski, and D.B. Considine, Simulation of stratospheric tracers using an improved empirically based two-dimensional model transport formulation, *J. Geophys. Res., 104*, 23,911-23,934, 1999.

Garcia, R.R., and S. Solomon, A numerical model of the zonally averaged dynamical and chemical structure of the middle atmosphere, *J. Geophys. Res., 88*, 1379-1400, 1983.

Garcia, R.R., T.J. Dunkerton, R.S. Lieberman, and R.A. Vincent, Climatology of the semiannual oscillation of the tropical middle atmosphere, *J. Geophys. Res., 102*, 26,019-26,032, 1997.

Gray, L.J., and J.A. Pyle, Two-dimensional model studies of equatorial dynamics and tracer distributions, *Q.J.R. Meteorol. Soc., 113*, 635-651, 1987.

Gray, L.J., and J.A. Pyle, A two-dimensional model of the quasi-biennial oscillation of ozone, *J. Atmos. Sci., 46*, 203-220, 1989.

Gray, L.J., and M.P. Chipperfield, On the interannual variability of trace gases in the middle atmosphere, *Geophys. Res. Lett., 17*, 933-936, 1990.

Gray, L.J., and T.J. Dunkerton, The role of the seasonal cycle in the quasi-biennial oscillation of ozone, *J. Atmos. Sci., 47*, 2429-2451, 1990.

Gray, L.J., and S. Ruth, The modeled latitudinal distribution of the ozone quasi-biennial oscillation using observed equatorial winds, *J. Atmos. Sci., 50*, 1033-1046, 1993.

Gray, L.J., and J.M. Russell III, Interannual variability of trace gases in the subtropical winter stratosphere, *J. Atmos. Sci., 56*, 977-993, 1999.

Hall, T.M., D.W. Waugh, K.A. Boering, and R.A. Plumb, Evaluation of transport in stratospheric models, *J. Geophys. Res., 104*, 18815-18839, 1999.

Hamilton, K., R.J. Wilson, and R.S. Hemler, Middle atmosphere simulated with high vertical and horizontal resolution versions of a GCM: Improvements in the cold pole bias and generation of a QBO-like oscillation in the tropics, *J. Atmos. Sci., 56*, 3829-3846, 1999.

Hasebe, F., Quasi-biennial oscillations of ozone and diabatic circulation in the equatorial stratosphere, *J. Atmos. Sci., 51*, 729-745, 1994.

Holton, J.R., and R.S. Lindzen, An updated theory for the quasi-biennial cycle of the tropical stratosphere, *J. Atmos. Sci., 29*, 1076-1080, 1972.

Holton, J.R., and H.C. Tan, The influence of the equatorial quasi-biennial oscillation on the global circulation at 50 mb, *J. Atmos. Sci., 37*, 2200-2208, 1980.

Holton, J.R., and X. Zhu, A further study of gravity wave induced drag and diffusion in the mesosphere, *J. Atmos. Sci., 41*, 2653-2662, 1984.

Huang, T.Y.W., and A.K. Smith, The mesospheric diabatic circulation and the parameterized thermal effect of gravity wave breaking on the circulation, *J. Atmos. Sci., 48*, 1093-1111, 1991.

Jackman, C.H., A.R. Douglass, R.B. Rood, R.D. McPeters, and P.E. Meade, Effect of solar

proton events on the middle atmosphere during the past two solar cycles as computed using a two-dimesional model, *J. Geophys. Res., 95*, 7417-7428, 1990.

Jackman, C.H., A.R. Douglass, S. Chandra, R.S. Stolarski, J.E. Rosenfield, J.A. Kaye, and E.R. Nash, Impact of interannual variability (1979-1986) of transport and temperature on ozone as computed using a two-dimensional photochemical model, *J. Geophys. Res., 96*, 5073-5079, 1991.

Jackman, C.H., E.L. Fleming, S. Chandra, D.B. Considine, and J.E. Rosenfield, Past, present, and future modeled ozone trends with comparisons to observed trends, *J. Geophys. Res., 101*, 28753-28767, 1996.

Jones, D.B.A., H.R. Schneider, and M.B. McElroy, Effects of the quasi-biennial oscillation on the zonally averaged transport of tracers, *J. Geophys. Res., 103*, 11235-11249, 1998.

Kennaugh, R., S. Ruth, and L.J. Gray, Modeling quasi-biennial variability in the semiannual double peak, *J. Geophys. Res., 102*, 16169-16187, 1997.

Kinnersley, J.S., and K.K. Tung, Modeling the global interannual variability of ozone due to the equatorial QBO and to extratropical planetary wave activity, *J. Atmos. Sci., 55*, 1417-1428, 1998.

Kinnersley, J.S., and K.K. Tung, Mechanisms for the extratropical QBO in circulation and ozone, *J. Atmos. Sci., 56*, 1942-1962, 1999.

Lait, L.R., M.R. Schoeberl, and P.A. Newman, Quasi-biennial modulation of the Antarctic ozone depletion, *J. Geophys. Res., 94*, 11,559-11,571, 1989.

Lindzen, R. S., Turbulence and stress owing to gravity wave and tidal breakdown, *J. Geophys. Res., 86*, 9707-9714, 1981.

Lindzen, R. S., and J.R. Holton, A theory of the quasi-biennial oscillation, *J. Atmos. Sci., 25*, 1095-1107, 1968.

Ling, X.-D., and J. London, The quasi-biennial oscillation of ozone in the tropical middle stratosphere: A one-dimensional model, *J. Atmos. Sci., 43*, 3122-3137, 1986.

Minschwaner, K., R.J. Salawitch, and M.B. McElroy, Absorption of solar radiation by O_2: Implications for O_3 and lifetimes of N_2O, $CFCl_3$, and CF_2Cl_2, *J. Geophys. Res., 98*, 10,543-10,561, 1993.

Nagashima, T., M. Takahashi, and F. Hasebe, The first simulation of an ozone QBO in a general circulation model, *Geophys. Res. Lett., 25*, 3131-3134, 1998.

Nash, J., Extension of explicit radiance observations by the stratospheric sound unit into the lower stratosphere and lower mesosphere, *Q.J.R. Meteorol. Soc., 114*, 1153-1171, 1988.

Naujokat, B., An update of the observed quasi-biennial oscillation of the stratospheric winds over the Tropics, *J. Atmos. Sci., 43*, 1873-1877, 1986.

Newell, R.E., J.W. Kidson, D.G. Vincent, and G.J. Boer, *The General Circulations of the Tropical Atmosphere*, vol. 2, chapter 7, MIT Press, Cambridge, Mass., 1974.

Niwano, M., and M. Shiotani, Quasi-biennial oscillation in vertical velocity inferred from trace gas data in the equatorial lower stratosphere, *J. Geophys. Res., 106*, 7281-7290, 2001.

Ortland, D.A., W.R. Skinner, P.B. Hays, M.D. Burrage, R.S. Lieberman, A.R. Marshall, D.A. Gell, Measurements of stratospheric winds by the high resolution Doppler imager, *J. Geophys. Res., 101*, 10,351-10,363, 1996.

O'Sullivan, D., and T.J. Dunkerton, The influence of the quasi-biennial oscillation on global constituent distributions, *J. Geophys. Res., 102*, 21,731-21,743, 1997.

Randel, W.J., and J.B. Cobb, Coherent variations of monthly mean total ozone and lower stratospheric temperature, *J. Geophys. Res., 99*, 5433-5447, 1994.

Randel, W.J., and R.R. Garcia, Application of a planetary wave breaking parameterization to stratospheric circulation statistics, *J. Atmos. Sci., 51*, 1157-1168, 1994.

Randel, W.J., and F. Wu, Isolation of the ozone QBO in SAGE II data by singular-value decomposition, *J. Atmos. Sci., 53*, 2546-2559, 1996.

Randel, W.J., B.A. Boville, J.C. Gille, P.L. Bailey, S.T. Massie, J.B. Kumer, J.L. Mergenthaler, and A.E. Roche, Simulation of stratospheric N_2O in the NCAR CCM2: Comparison with CLAES data and global budget analysis, *J. Atmos. Sci., 51*, 2834-2845, 1994.

Randel, W.J., F. Wu, J.M. Russell III, A. Roche, and J.W. Waters, Seasonal cycles and QBO variations in stratospheric CH_4 and H_2O observed in UARS HALOE data, *J. Atmos. Sci., 55*, 163-185, 1998.

Randel, W.J., F. Wu, R. Swinbank, J. Nash, and A. O'Neill, Global QBO circulation derived from UKMO stratospheric analyses, *J. Atmos. Sci., 56*, 457-474, 1999.

Reed, R.J., W.J. Campbell, L.A. Rasmussen, and D.G. Rodgers, Evidence of a downward-propagating annnual wind reversal in the equatorial stratosphere, *J. Geophys. Res., 66*, 813-818, 1961.

Reed, R.J., A tentative model of the 26 month oscillation in tropical latitudes, *Q.J.R. Meteorol. Soc., 90*, 665-674, 1964.

Rosenfield, J.E., P.A. Newman, and M.R. Schoeberl, Computations of diabatic descent in the stratospheric polar vortex, *J. Geophys. Res., 99*, 16677-16689, 1994.

Ruth, S., R. Kennaugh, L.J. Gray, and J.M. Russell III, Seasonal, semiannual, and interannual variability seen in measurements of methane made by the UARS Halogen Occultation Experiment, *J. Geophys. Res., 102*, 16189-16199, 1997.

Sander, S.P., et al., Chemical kinetics and photochemical data for use in stratospheric modeling, Supplement to Evaluation 12: Update of key reactions, Evaluation number 13, *JPL Publ., 00-3*, 74 pp., 2000.

Schoeberl, M.R., D.F. Strobel, and J.P. Apruzese, A numerical model of gravity wave breaking and stress in the mesosphere, *J. Geophys. Res., 88*, 5249-5259, 1983.

Stolarski, R.S., S.M. Frith, R.D. McPeters, L. Flynn, and G. Labow, A 20-year data set for total column ozone derived from multiple satellite instruments, *J. Geophys. Res.*, (in preparation), 2001.

Tung, K.K., and H. Yang, Global QBO in circulation and ozone, Part I: Reexamination of observational evidence, *J. Atmos. Sci., 51*, 2699-2707, 1994.

Veryard, R.G., and R.A. Ebdon, Fluctuations in tropical stratospheric winds, *Meteor. Mag., 90*, 125-143, 1961.

Wallace, J.M., R.L. Panetta, and J. Estberg, Representation of the equatorial stratospheric quasi-biennial oscillation in EOF phase space, *J. Atmos. Sci., 50*, 1751-1762, 1993.

World Meteorological Organization (WMO), Scientific Assessment of Ozone Depletion: 1998, *Rep. 44* Global Ozone Research and Monitoring Project, Geneva, 1999.

Zawodny, J.M, and M.P. McCormick, Stratospheric aerosol and gas experiment II measurements of the quasi-biennial oscillations in ozone and nitrogen dioxide, *J.*

Geophys. Res., *96*, 9371-9377, 1991.

This manuscript was prepared with the AGU LaTeX macros v3.0.

Figure Captions

Figure 1. Time series of the equatorial residual mean vertical velocity ($\bar{w}^*$) for model scenario A for the altitudes indicated.

Figure 2. Equatorial time-height sections of the model residual mean vertical velocity ($\bar{w}^*$) for model scenario A. Shown are the time series in which the trend and seasonal cycles have been removed by regression analysis and then smoothed by 2 passes of a 3-point running average (top), and the QBO statistical fit to the detrended and deseasonlized time series (bottom). Contour intervals are 0.05 mm/sec. Negative anomalies are shaded. See text for details of the QBO fitting procedure.

Figure 3. Equatorial vertical profiles of the QBO amplitude and phase of the residual mean vertical velocity ($\bar{w}^*$) from model scenarios A (solid line), B (dashed-dotted line), and C (dotted line). See text for details concerning the QBO statistical fitting.

Figure 4. Time series of CH_4 from UARS HALOE version 19 data (red dashed line-asterisk), and model scenarios A (solid line), B (dashed-dotted line), and C (dotted line) for 10°S-10°N at the altitudes indicated.

Figure 5. Time series of detrended and deseasonalized CH_4 from UARS HALOE version 19 data (red dashed line-asterisk), and model scenarios A (solid line), B (dashed-dotted line), and C (dotted line) for 10°S-10°N at the altitudes indicated. The trend and seasonal cycles have been removed by regression analysis. A solar cycle component has also been removed from the HALOE data.

Figure 6. Vertical profiles of the QBO amplitude and phase of CH_4 from HALOE version 19 (red dashed line-asterisk), and model scenarios A (solid line), B (dashed-dotted line), and C (dotted line) for 10°S-10°N. See text for details concerning the QBO statistical fitting.

Figure 7. Time series of O_3 from UARS HALOE version 19 data (red dashed line-asterisk), MLS version 5 data (green dashed line-triangles), and model scenarios A (solid line), B (dashed-dotted line), and C (dotted line) for 10°S-10°N at the altitudes indicated.

Figure 8. Time series of detrended and deseasonalized O_3 from UARS HALOE version 19 data (red dashed line-asterisk), MLS version 5 data (green dashed line-triangles), and model scenarios A (solid line), B (dashed-dotted line), and C (dotted line) for 10°S-10°N at the altitudes indicated. The trend and seasonal cycles have been removed by regression analysis. A solar cycle component has also been removed from the HALOE and MLS data.

Figure 9. Eqautorial time-height sections of the QBO statistical fit to the detrended and deseasonlized O_3 time series for 10°S-10°N. Shown are the MLS version 5 data (top), HALOE version 19 data (middle), and model scenario A (bottom). The contour interval is 0.1 ppmv and negative anomalies are shaded. See text for details of the QBO fitting procedure.

Figure 10. Vertical profiles of the QBO amplitude and phase of O_3 from HALOE version 19 (red dashed line-asterisk), and model scenarios A (solid line), B (dashed-dotted line), and C (dotted line) for 10°S-10°N. The amplitudes and phases are determined from the QBO statistical fitted time series shown in Figure 9. See text for details concerning the QBO statistical fitting.

Figure 11. Time series of detrended and deseasonalized O_3 from model scenarios A (black line), D (red line), E (blue line), and F (purple dashed-dotted line) for 10°S-10°N at the altitudes indicated. The trend and seasonal cycles have been removed by regression analysis.

Figure 12. Vertical profiles of the QBO amplitude and phase of O_3 from model scenarios A (black line), D (red line), E (blue line), and F (purple dashed-dotted line) for 10°S-10°N. See text for details concerning the QBO statistical fitting.

Figure 13. Top panel shows time series of total column ozone from the TOMS/SBUV merged data set (red dashed line-asterisk), and model scenarios A (solid line), B (dashed-dotted line), and C (dotted line) for 10°S-10°N. Bottom panel shows the time series with the trend and seasonal cycles removed by regression analysis. A solar cycle component has also been removed from the TOMS/SBUV data.

Figure 14. Vertical profiles of mean age of air at 10°S-10°N from the model (scenario A) averaged over 1993-2000 (solid line), the model interannual range during 1993-2000 (dashed lines), and the model average for February and November 1997 (dotted line). Also shown are the mean age determined from OMS balloon measurements of CO_2 (red pluses) and SF_6 (red triangles) taken during February and November 1997 at 7°S, and ER-2 aircraft measurements of CO_2 (blue asterisk) and SF_6 (blue square) at 20 km averaged over 10°S-10°N during 1992-1997. Ages are taken relative to the tropical tropopause.

Table 1. Description of model simulations

Scenario	Description
A	temperature and all transport components varied interannually
B	scenario A + climatological O_3 and H_2O used in diabatic heating rates
C	scenario A + QBO temperature anomalies increased by 40%
D	interannual transport from scenario A + climatological temperatures used in reaction rates
E	climatological transport + interannual temperatures from scenario A used in reaction rates
F	scenario A + all odd nitrogen species kept constant

Table 2. Total Ozone QBO Signal Amplitude and Phase for 10°S-10°N

Scenario	Amplitude (DU)	Phase (fractional QBO cycle)
A	2.1	0.28
B	5.0	0.32
C	3.3	0.31
D	2.6	0.27
E	0.5	0.74
F	2.4	0.26
TOMS/SBUV	6.3	0.28

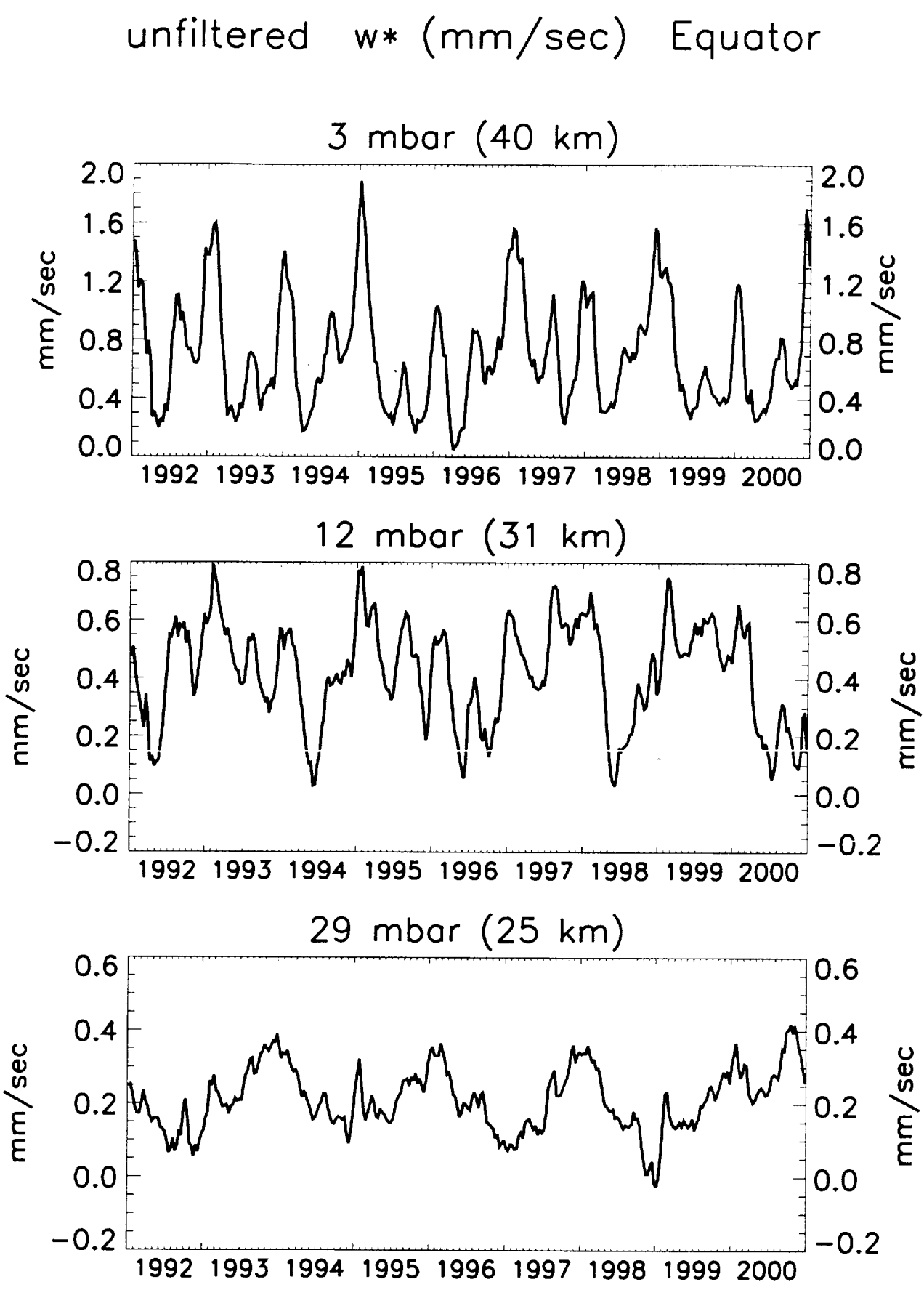
unfiltered w* (mm/sec) Equator
3 mbar (40 km)
12 mbar (31 km)
29 mbar (25 km)
mm/sec
2.0
1.6
1.2
0.8
0.4
0.0
0.6
0.2
−0.2
1992 1993 1994 1995 1996 1997 1998 1999 2000

Figure 1

Equator

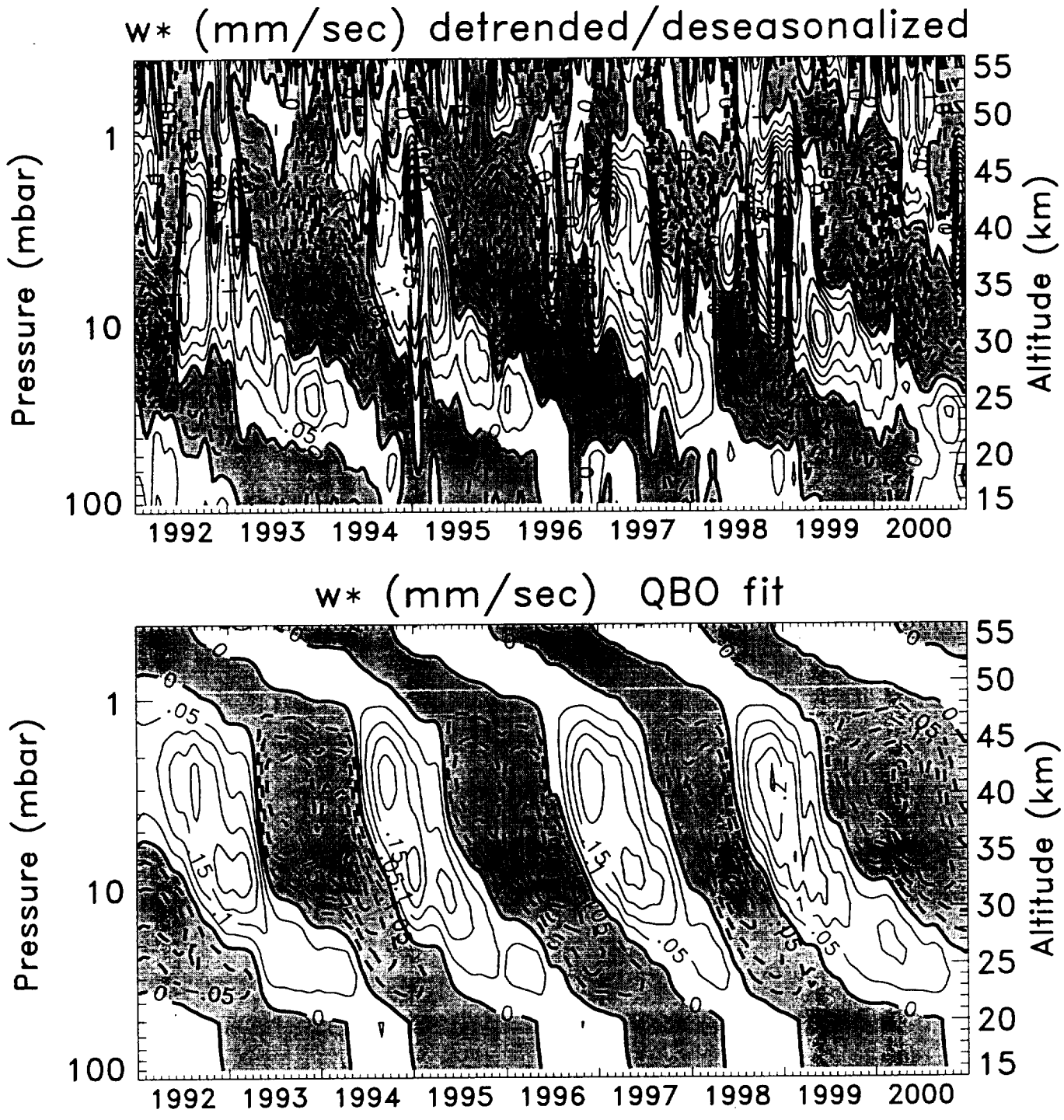

Figure 2

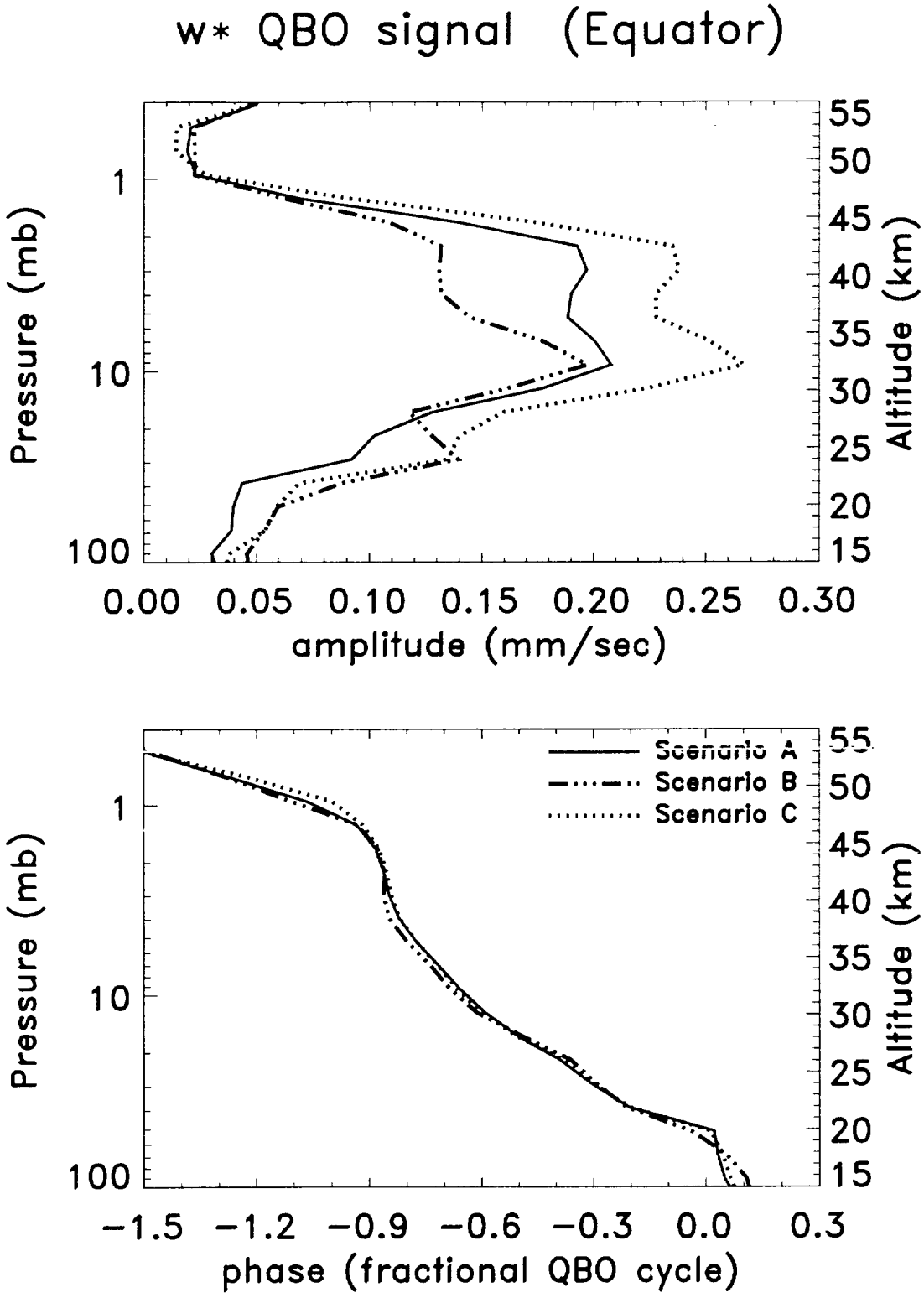
w* QBO signal (Equator)
Pressure (mb)
1
10
100
55
50
45
40
35
30
25
20
15
Altitude (km)
0.00 0.05 0.10 0.15 0.20 0.25 0.30
amplitude (mm/sec)
Scenario A
Scenario B
Scenario C
−1.5 −1.2 −0.9 −0.6 −0.3 0.0 0.3
phase (fractional QBO cycle)

Figure 3

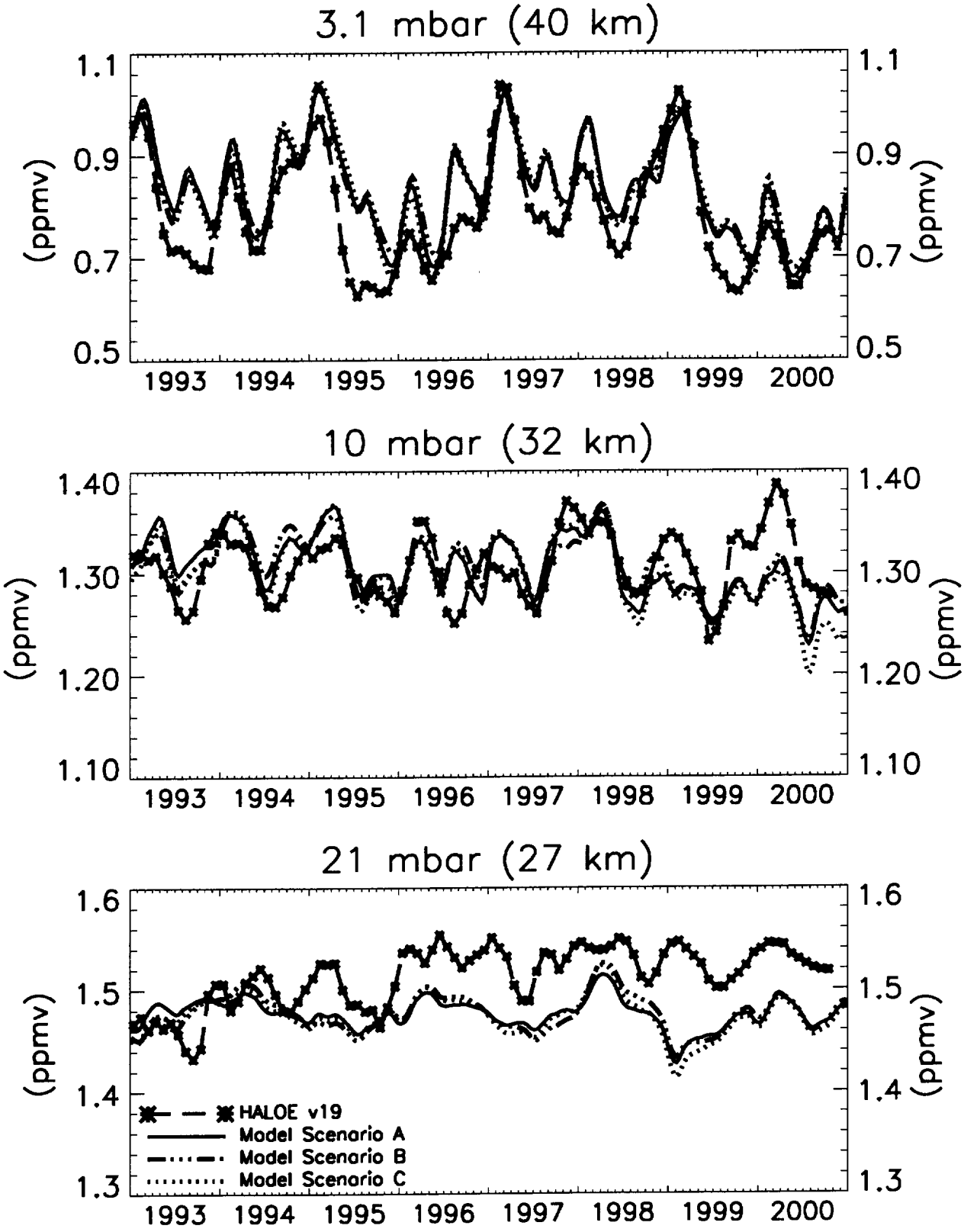
unfiltered CH_4 10°S–10°N
3.1 mbar (40 km)
10 mbar (32 km)
21 mbar (27 km)
(ppmv)
1.1
0.9
0.7
0.5
1.40
1.30
1.20
1.10
1.6
1.5
1.4
1.3
1993
1994
1995
1996
1997
1998
1999
2000
HALOE v19
Model Scenario A
Model Scenario B
Model Scenario C

Figure 4

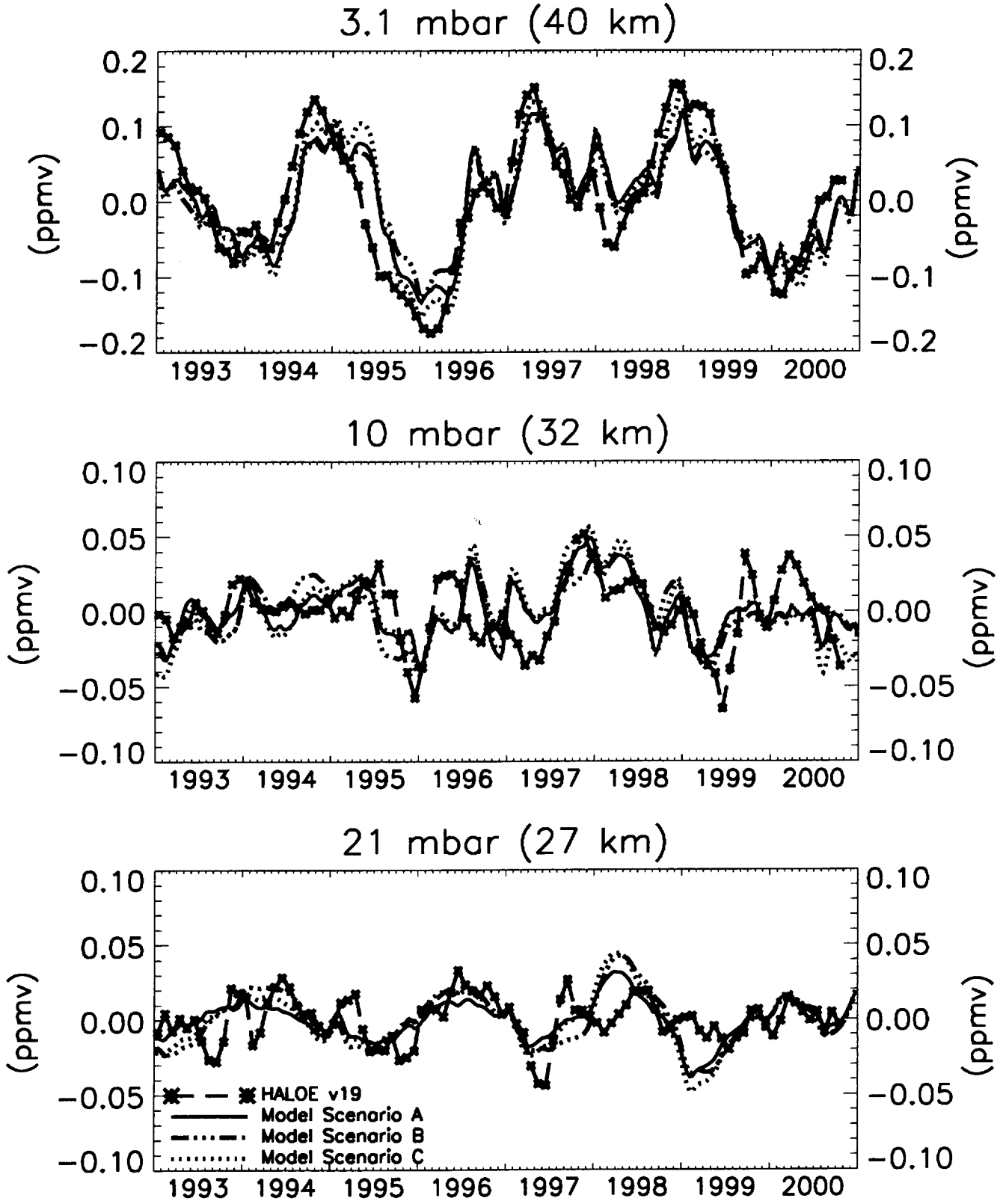
detrended/deseasonalized CH_4 10°S–10°N
3.1 mbar (40 km)
10 mbar (32 km)
21 mbar (27 km)
(ppmv)
0.2
0.1
0.0
−0.1
−0.2
0.10
0.05
0.00
−0.05
−0.10
1993
1994
1995
1996
1997
1998
1999
2000
HALOE v19
Model Scenario A
Model Scenario B
Model Scenario C

Figure 5

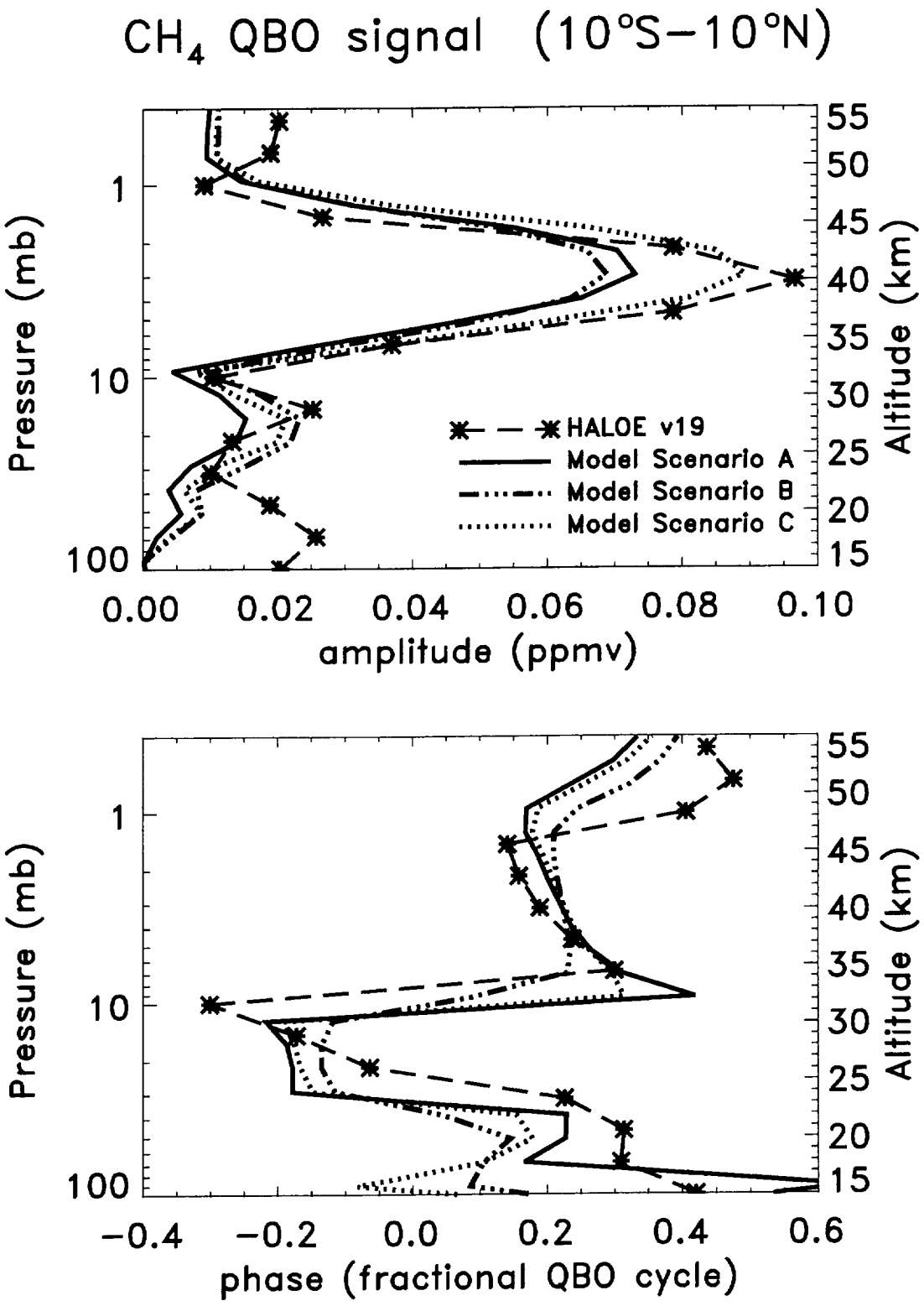
CH4 QBO signal (10°S–10°N)
Pressure (mb)
1
10
100
Altitude (km)
55
50
45
40
35
30
25
20
15
HALOE v19
Model Scenario A
Model Scenario B
Model Scenario C
0.00
0.02
0.04
0.06
0.08
0.10
amplitude (ppmv)
−0.4
−0.2
0.0
0.2
0.4
0.6
phase (fractional QBO cycle)

Figure 6

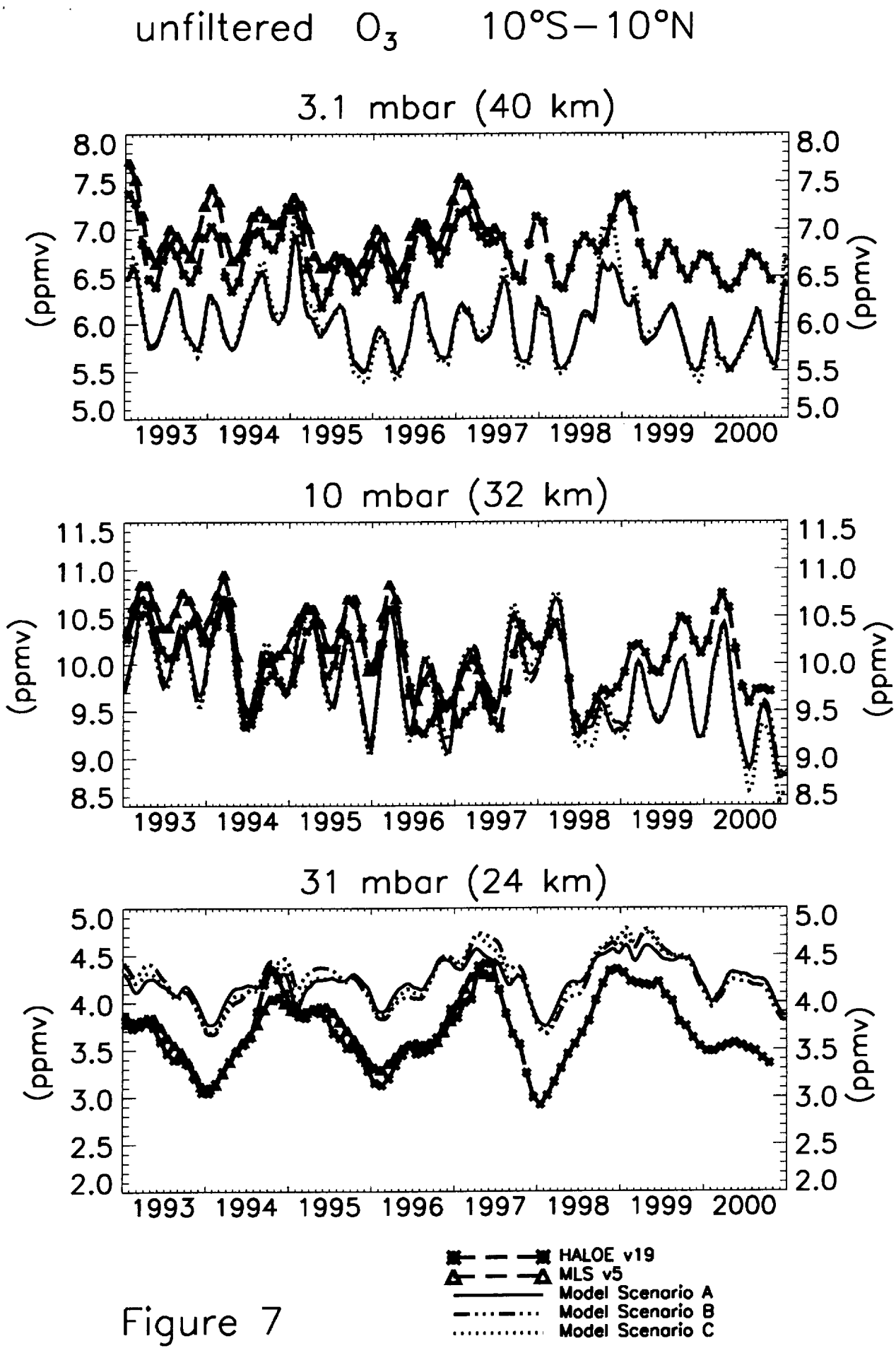
unfiltered O_3 10°S–10°N
3.1 mbar (40 km)
10 mbar (32 km)
31 mbar (24 km)
(ppmv)
1993 1994 1995 1996 1997 1998 1999 2000
HALOE v19
MLS v5
Model Scenario A
Model Scenario B
Model Scenario C

Figure 7

detrended/deseasonalized O_3 10°S–10°N

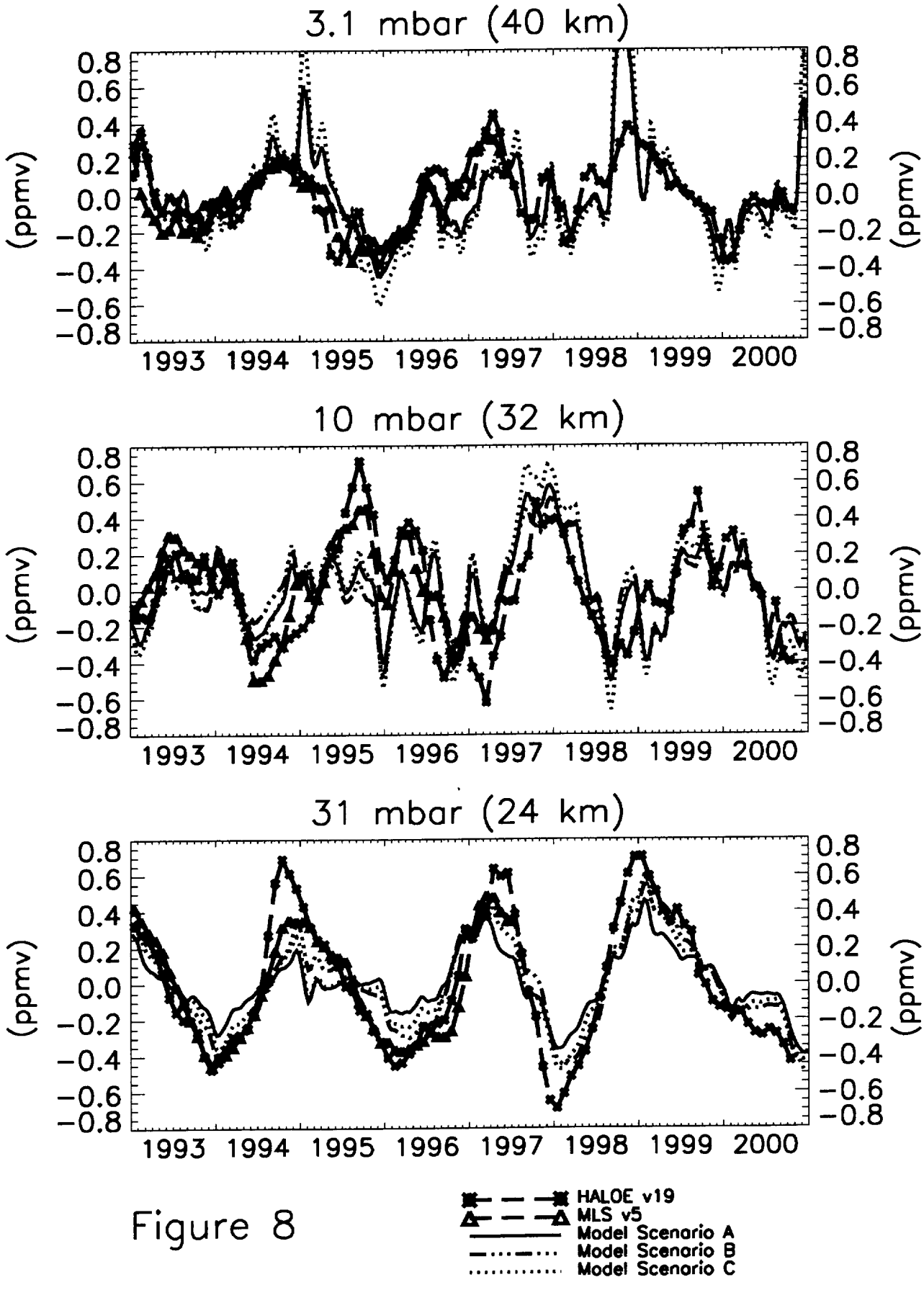

Figure 8

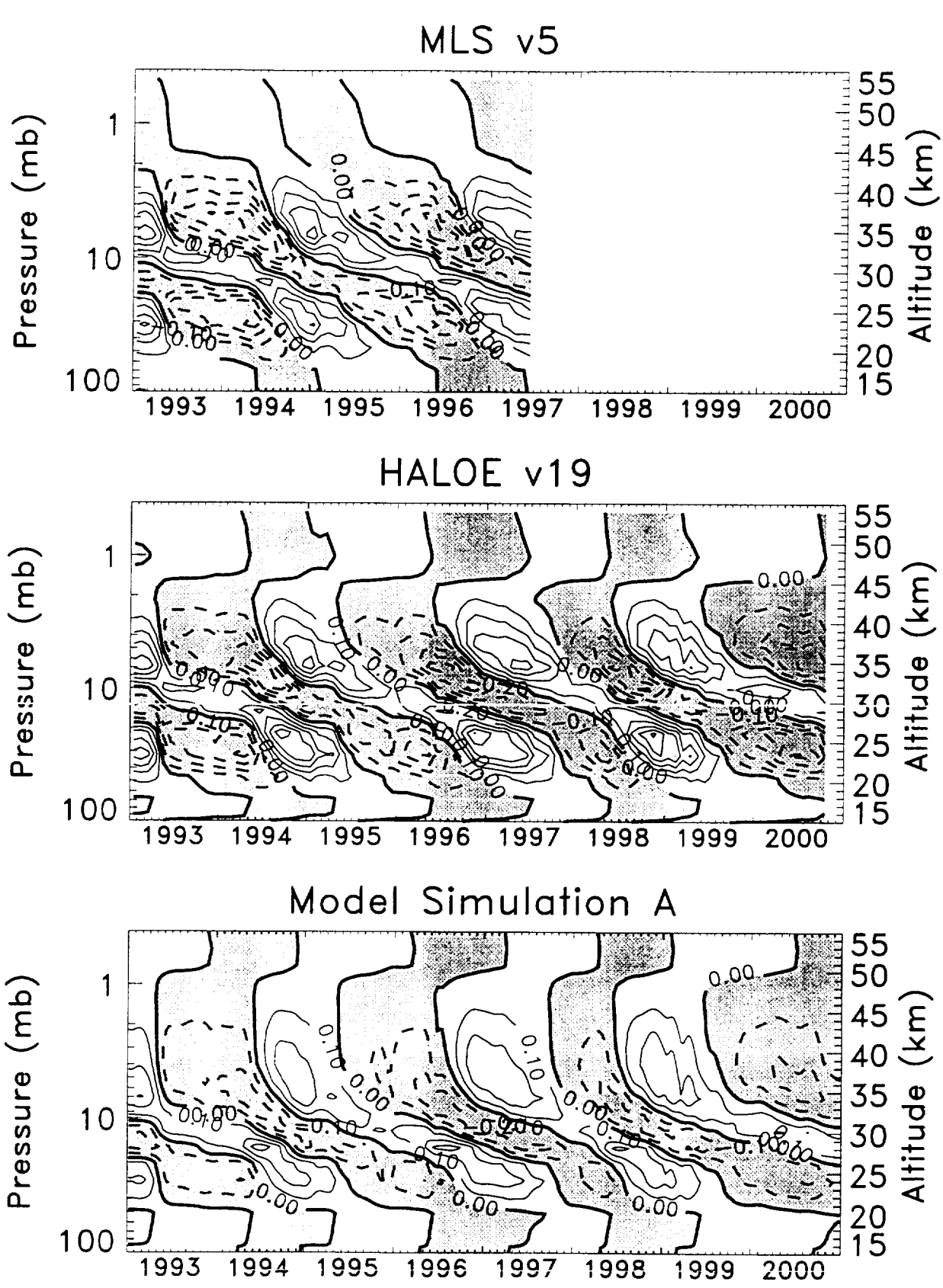
O_3 (ppmv) 10°S–10°N QBO FIT (EOF1+EOF2)
MLS v5
HALOE v19
Model Simulation A
Pressure (mb)
Altitude (km)
1
10
100
55
50
45
40
35
30
25
20
15
1993
1994
1995
1996
1997
1998
1999
2000

Figure 9

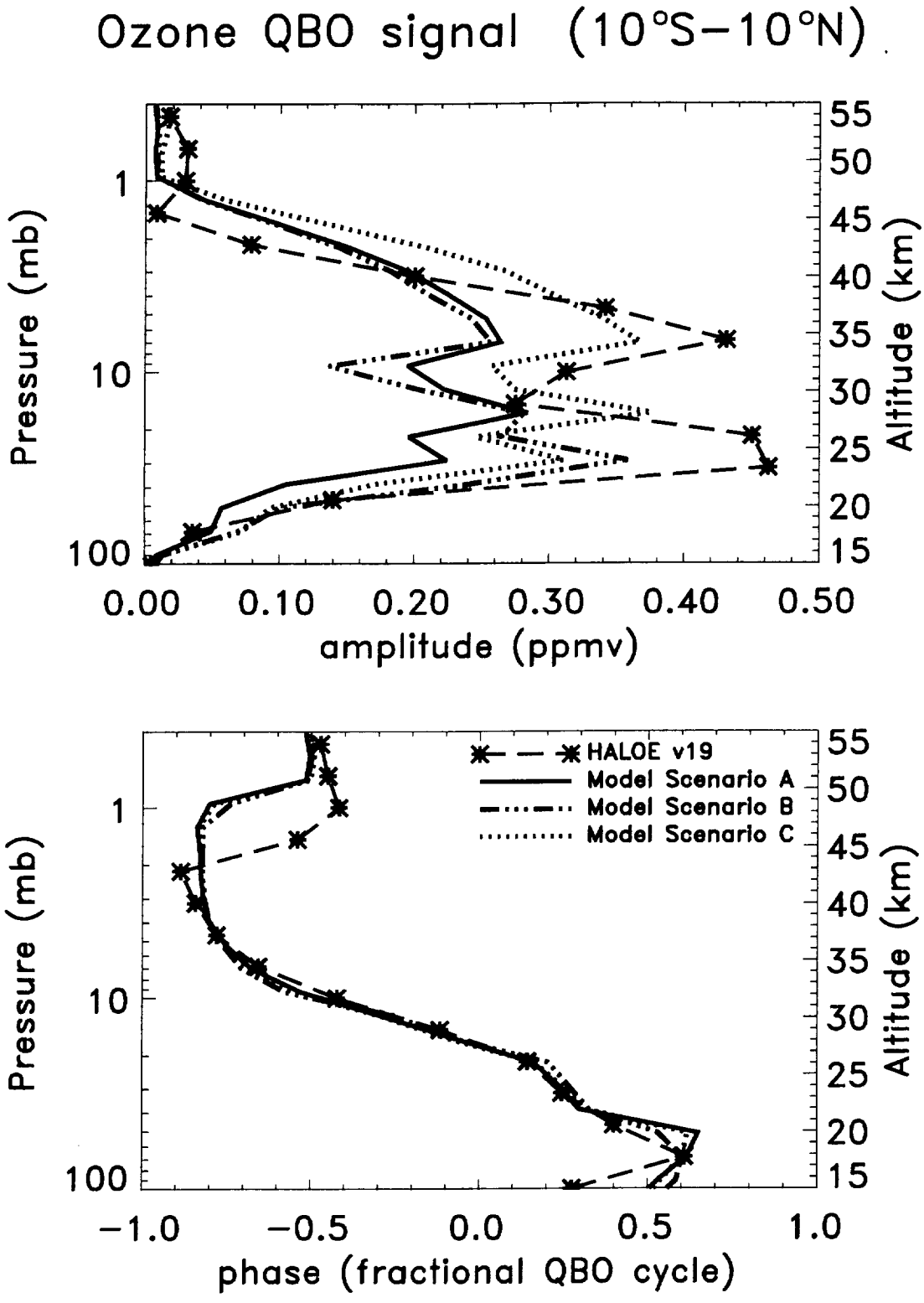
Ozone QBO signal (10°S–10°N)
Pressure (mb)
1
10
100
55
50
45
40
35
30
25
20
15
Altitude (km)
0.00
0.10
0.20
0.30
0.40
0.50
amplitude (ppmv)
HALOE v19
Model Scenario A
Model Scenario B
Model Scenario C
−1.0
−0.5
0.0
0.5
1.0
phase (fractional QBO cycle)

Figure 10

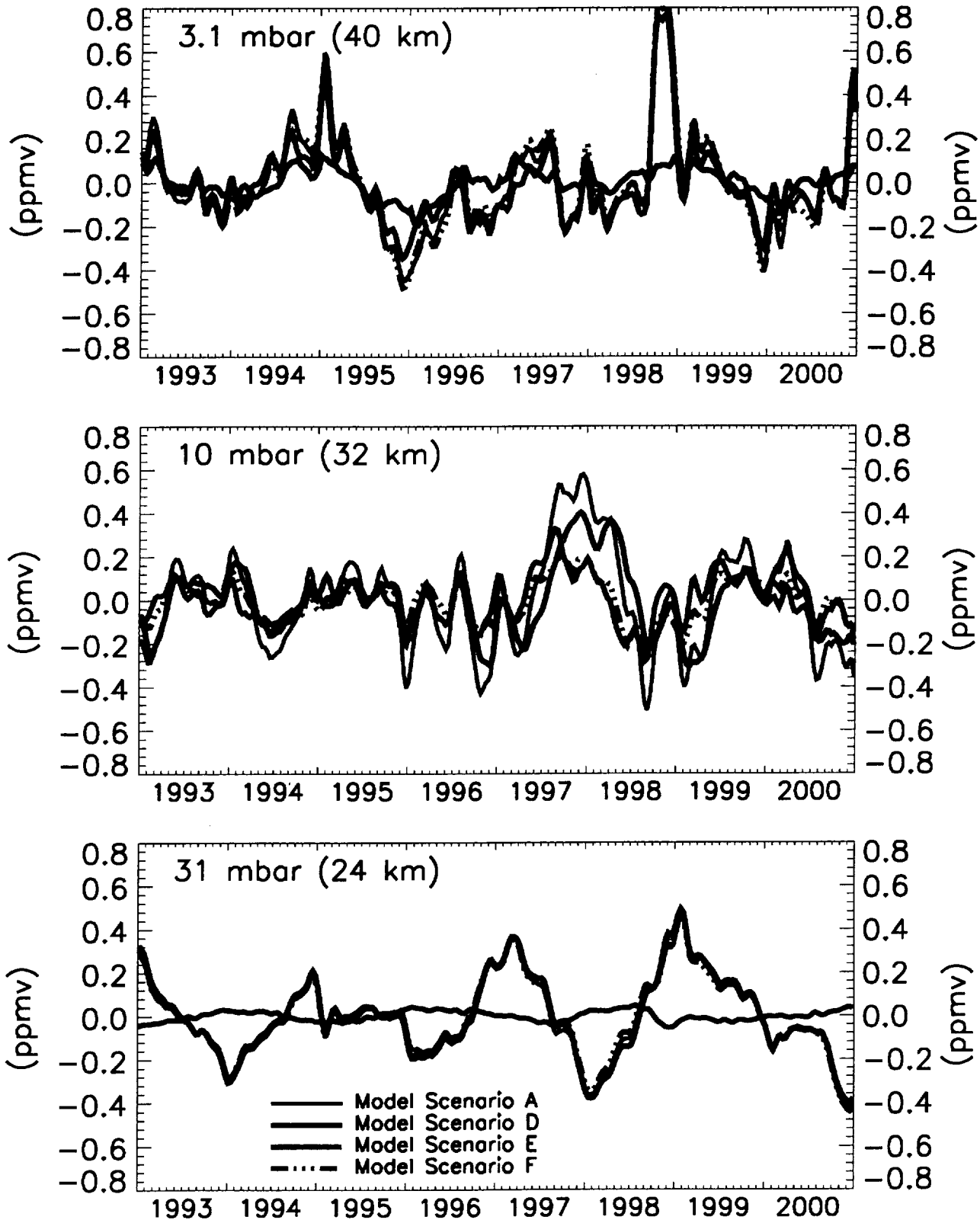
detrended/deseasonalized O_3 10°S–10°N
3.1 mbar (40 km)
10 mbar (32 km)
31 mbar (24 km)
(ppmv)
0.8
0.6
0.4
0.2
0.0
−0.2
−0.4
−0.6
−0.8
1993
1994
1995
1996
1997
1998
1999
2000
Model Scenario A
Model Scenario D
Model Scenario E
Model Scenario F

Figure 11

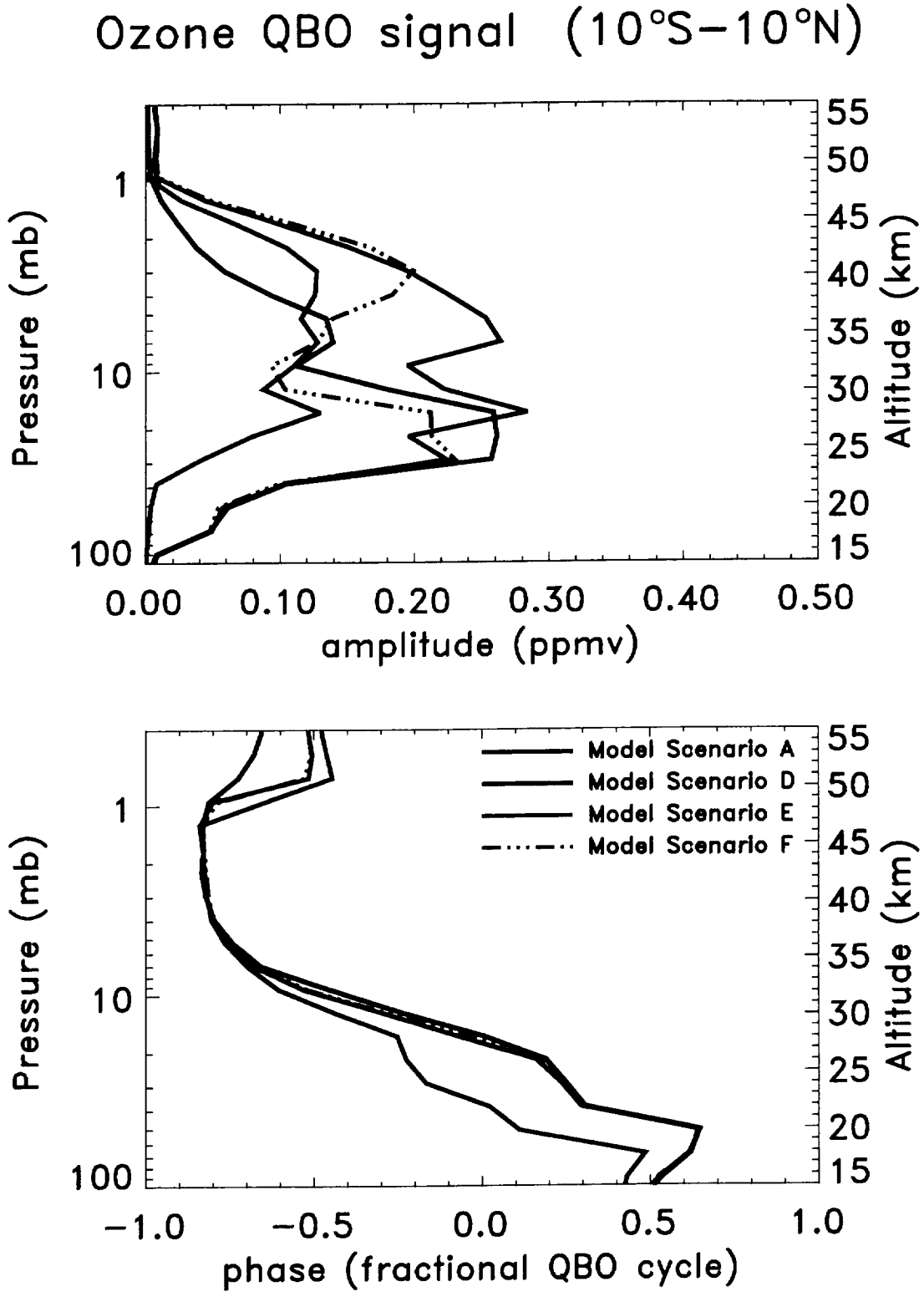
Ozone QBO signal (10°S–10°N)
Pressure (mb)
1
10
100
55
50
45
40
35
30
25
20
15
Altitude (km)
0.00
0.10
0.20
0.30
0.40
0.50
amplitude (ppmv)
Model Scenario A
Model Scenario D
Model Scenario E
Model Scenario F
−1.0
−0.5
0.0
0.5
1.0
phase (fractional QBO cycle)

Figure 12

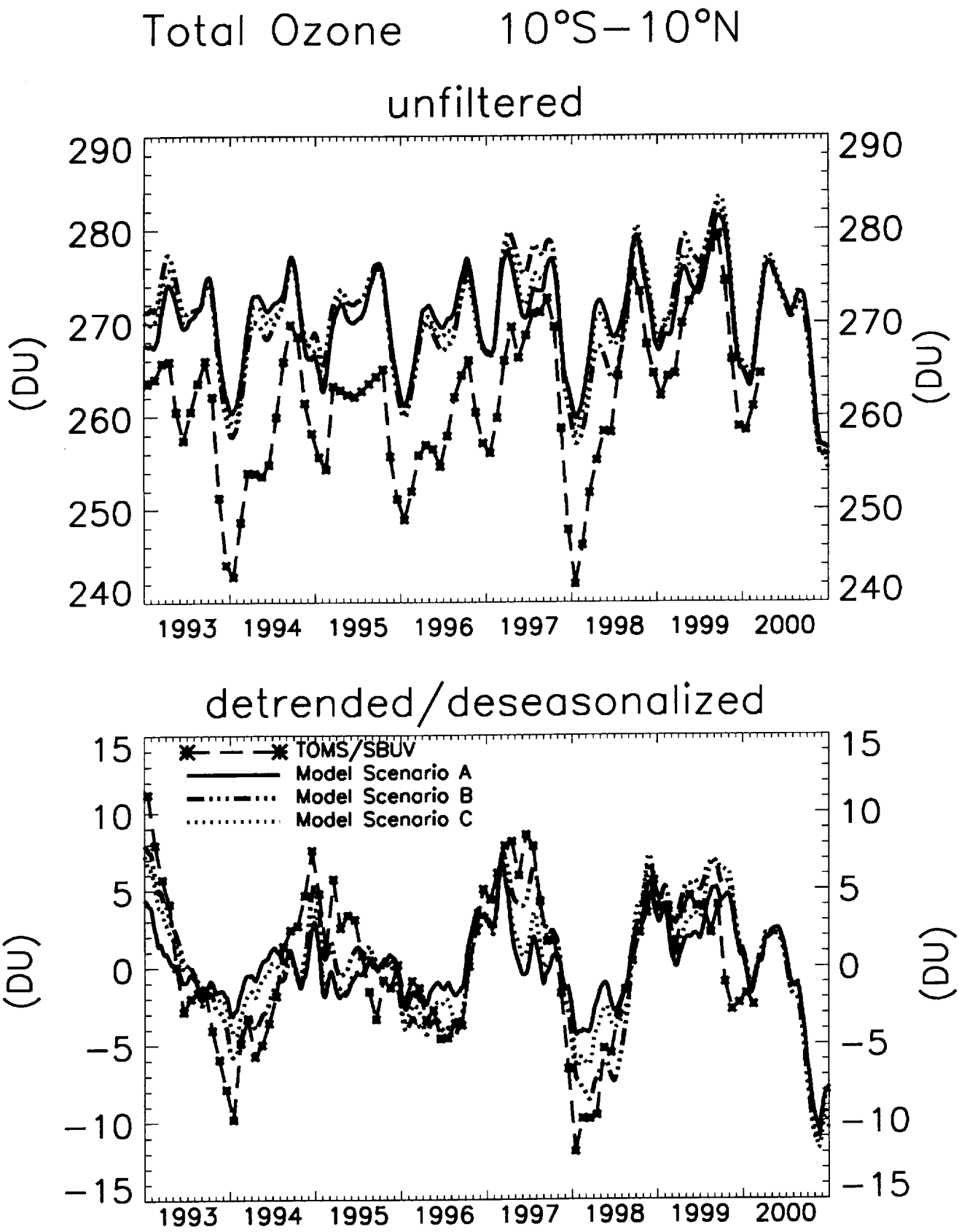
Total Ozone 10°S–10°N
unfiltered
290
280
270
260
250
240
(DU)
1993
1994
1995
1996
1997
1998
1999
2000
detrended/deseasonalized
TOMS/SBUV
Model Scenario A
Model Scenario B
Model Scenario C
15
10
5
0
−5
−10
−15
(DU)

Figure 13

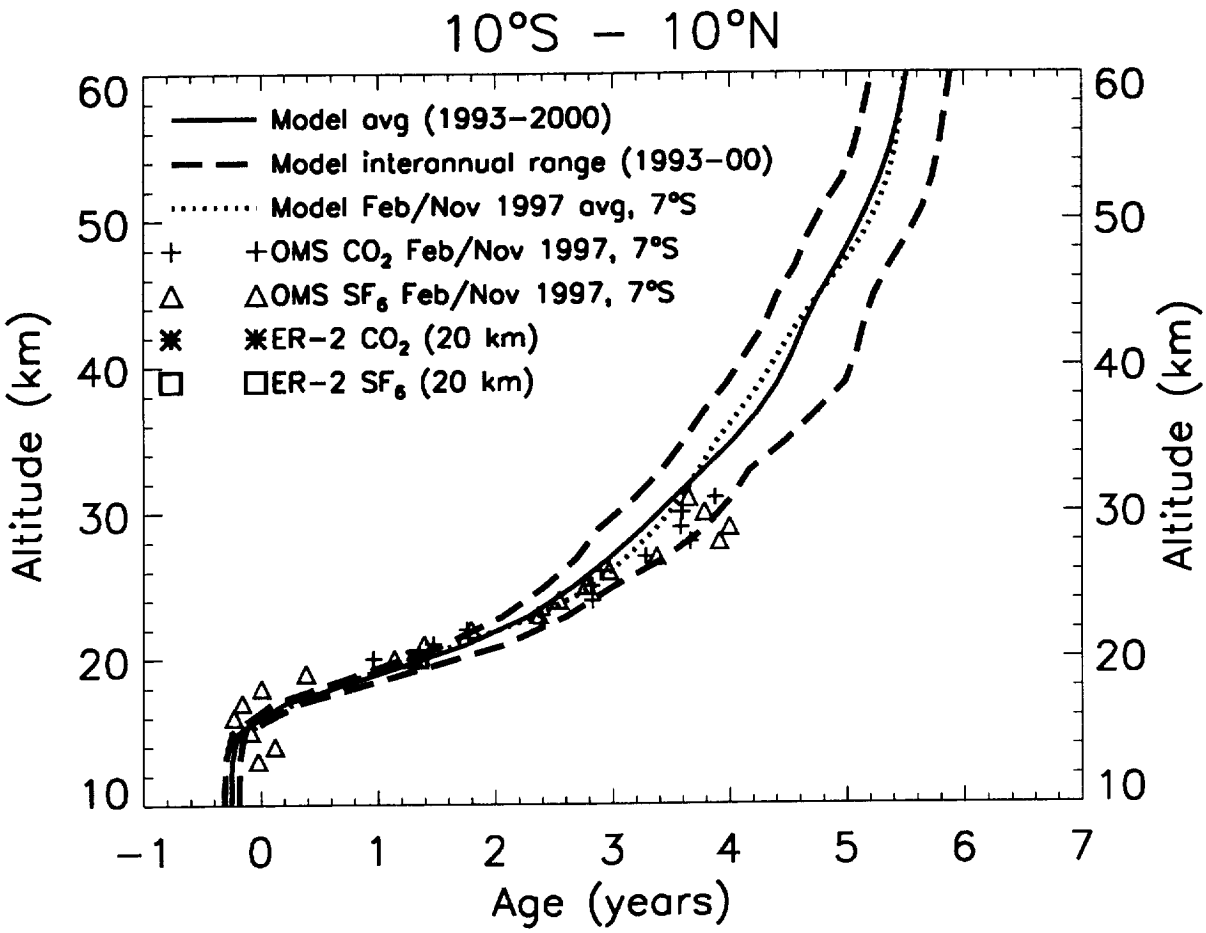
10°S – 10°N
Model avg (1993–2000)
Model interannual range (1993–00)
Model Feb/Nov 1997 avg, 7°S
+OMS CO_2 Feb/Nov 1997, 7°S
ΔOMS SF_6 Feb/Nov 1997, 7°S
✱ER–2 CO_2 (20 km)
□ER–2 SF_6 (20 km)
Altitude (km)
Age (years)
60
50
40
30
20
10
–1
0
1
2
3
4
5
6
7

Figure 14

Popular Summary

"Two-dimensional model simulations of interannual variability in the tropical stratosphere", by E.L. Fleming, C.H. Jackman, D.B. Considine, and J. Rosenfield

Atmospheric chemical models are widely used for scientific studies and international assessments that advance our understanding of the natural and man-made influences on the Earth's ozone layer. Two types of models are generally used for this work: three-dimensional (3-D) longitude-latitude-height models, and two-dimensional (2-D) latitude-height models in which the longitudinal variations have been averaged. Compared to 3-D models, two-dimensional models are less computationally intensive and provide a somewhat simpler framework for understanding the changes that influence the ozone layer. An important aspect of 2-D models is the proper treatment of both atmospheric chemical processes and atmospheric motions, or wind systems, which transport various chemical compounds, including ozone, around the globe. In the stratosphere, a region approximately 10-30 miles above the earth where the majority of the ozone resides, the atmospheric variability in the tropics is dominated by an approximate two year cycle, or quasi-biennial oscillation (QBO). It is important for 2-D models to adequately resolve the effects of the QBO to properly simulate long term changes to the ozone layer.

In this paper, we discuss techniques for incorporating the effects of the QBO in our NASA/GSFC 2-D model using a variety of meteorological data sets. We also investigate the relative roles of atmospheric motions and atmospheric chemical processes in determining the QBO effects on ozone. We then show numerous comparisons between the model simulations and observations of ozone and long-lived chemical compounds in the tropical stratosphere. The long-lived compounds, which are not strongly influenced by atmospheric chemical processes, are important as they act as tracers of the atmospheric motions as they move around the globe. These comparisons provide tests that show that the model simulates the effects of the QBO in the real atmosphere reasonably well. The success of this validation then increases the credibility of our model simulations of the long term natural and man-made influences on the ozone layer.